


Hadronic structure on the light front. III. The Hamiltonian, heavy quarkonia, spin, and orbit mixing

Edward Shuryak^{*} and Ismail Zahed[†]

Center for Nuclear Theory, Department of Physics and Astronomy, Stony Brook University,
Stony Brook, New York 11794–3800, USA

 (Received 15 August 2022; accepted 12 January 2023; published 24 February 2023)

This is the third paper on hadronic light-front wave functions. We derive a light-front Hamiltonian from first principles, using the key features of the QCD vacuum at low resolution. In the first approximation, it gives transverse oscillator and longitudinal harmonic modes, and yields the correct Regge trajectories. For heavy quarkonia, we compare its spectrum to that obtained from the usual Schrödinger equation in the rest frame. We use the same approach for light quarks, and investigate the role of confinement and chiral symmetry breaking in the quark-antiquark sector. We then study spin-spin and spin-orbit mixing, resulting in e.g. quadrupole moments of vector mesons. For the light mesons, we show how to extend the famed 't Hooft interaction to the light front, which solves the U(1) problem and helps produce a light pion. We use the ensuing light front wave functions to derive the pertinent parton distribution functions, parton amplitudes, and low energy constants.

DOI: [10.1103/PhysRevD.107.034025](https://doi.org/10.1103/PhysRevD.107.034025)

I. INTRODUCTION

The physics of hadrons is firmly based in quantum chromodynamics, a theory over half a century old. One might think that by now this subject has reached a solid degree of maturity with most issues settled. Yet persisting tension remains between the nonperturbative aspects of the theory and empirical measurements using inclusive and exclusive processes.

More specifically, first principle approaches—lattice and semiclassical—are focused on the ground state properties of the QCD vacuum, using Euclidean time formulation. Hadrons are then studied via certain correlation functions (a brief review will be given in the next subsection). However, a significant part of the experimental information—parton distribution functions (PDFs) used in deep inelastic inclusive processes, and distribution amplitudes (DAs) used for exclusive processes—are defined in the light-front kinematics, and therefore are not directly accessible by the Euclidean formulation. Only recently, the first attempt to formulate the appropriate kinematical limits [1] and use the lattice for calculating the PDFs [2,3] were carried out with some success.

Bringing the two sides of hadronic physics together is not just a technical issue related with kinematics. Even the main pillars of the theory—confinement and chiral symmetry breaking—become contentious. In particular, 60 years ago Nambu and Jona-Lasinio (NJL) [4] explained that pions are light because they are near-massless vacuum waves due to the spontaneous breaking of chiral symmetry. The mechanism creating the vacuum quark condensate and the ensuing organization using chiral perturbation theory have since been discussed and confirmed in countless papers.

More importantly, the QCD vacuum in the mesoscopic limit, reveals a multitude of multi-quark correlations captured by universal spectral fluctuations in the *zero mode zone* (ZMZ) [5]. They are analogous to the universal conductance fluctuations around Fermi surfaces in dirty metals [6]. We regard these mesoscopic fluctuations as strong evidence, in support of the topological origin of the spontaneous breaking of chiral symmetry in QCD. Most of the current hadronic models fail to reproduce these fluctuations.

And yet, parton dynamics is still treated as if the vacuum is “empty” and quarks are treated as massless. There are even suggestions that on the light front there are no condensates [7,8]. The pion was also suggested to be massless due to other reasons [9]. Recently these arguments were revisited [10], and “quasi-PDFs” have been calculated on the lattice [11] (and references therein), obviously with all nonperturbative effects included.

Still, there remains a significant gap between light-front observables used and hadronic spectroscopy (as well as atomic and nuclear ones): the former focuses on certain

^{*}edward.shuryak@stonybrook.edu

[†]ismail.zahed@stonybrook.edu

Published by the American Physical Society under the terms of the [Creative Commons Attribution 4.0 International license](https://creativecommons.org/licenses/by/4.0/). Further distribution of this work must maintain attribution to the author(s) and the published article's title, journal citation, and DOI. Funded by SCOAP³.

matrix elements (DAs, PDFs, transverse momentum distributions, etc.) rather than the wave functions, or the underlying Hamiltonian. This approach is entirely driven by information deduced from experiment.

Indeed, one can calculate various inclusive and exclusive reactions using DAs. But their number is in principle infinite, as there are unlimited number of operators. (The standard approach is to include only those with the smallest values of their *twist*, dimension minus spin, thereby limiting the discussion to the large Q^2 domain.) The normalization of the DAs is done via a number of empirical constants like f_π , f_ρ .

Hadronic spectroscopy, as in many other similar fields, goes in the opposite direction, from the underlying theory to effective Hamiltonians, to wave functions, to matrix elements. Indeed, one Hamiltonian produces many eigenstates, with well-defined wave functions, naturally normalized and mutually orthogonal. From them any number of matrix elements of interest can be calculated.

The light-front wave functions were classified in well-known papers such as [12], but hardly used. Only for the pion—a very special particle, a Nambu–Goldstone mode—there is determination of both of its components, from model-dependent Bethe–Salpeter equations [13,14], and from quasi-DAs in the instanton vacuum [15].

Model Hamiltonians were invented, but not related to the underlying physics. The spin-dependent forces—so important in spectroscopy—have not been included. In [16] we reviewed their perturbative and nonperturbative aspects in the rest frame, and in [17] we showed how to extend the nonperturbative contributions to the light front. (See also other papers in this series [18,19].)

In this paper, a comprehensive derivation of the perturbative spin contributions will be given using Wilson lines on the light front. When combined with the nonperturbative contributions from [17], it provides a first principle Hamiltonian on the light front. The spectroscopic implications of this Hamiltonian for heavy and light mesons will be investigated.

The organization of the paper is as follows: In Secs. II and III we give a first principle derivation of the light-front Hamiltonian, through an analytical continuation of pertinent Wilson loops from Euclidean to Minkowski signature. The derivation includes both the perturbative and nonperturbative gluonic contributions in the QCD vacuum at low resolution. In Sec. IV we limit the light-front Hamiltonian to the contributions stemming from confinement and Coulomb, and analyze their role on heavy quarkonia, with Upsilon as an example. In Sec. V we briefly review how parity is defined on the light front, and how it is used to organize the light-front wave functions for mesons. In Sec. VI we consider the mixing induced by the tensor contribution to the light-front Hamiltonian, onto heavy quarkonia. We show that the quadrupole moment of Upsilon on the light front is about comparable to the one extracted from other approaches both at rest and also on the light front. In Sec. VII, we consider the additional

mixing induced by spin-orbit coupling on the light front, and apply in this case to the light meson spectrum. In Sec. VIII we show how the subtle zero modes associated to tunneling through instantons in Euclidean signature are lifted to the light front, using the Lehmann-Symanzik-Zimmermann (LSZ) reduction in coordinate space. We use it to derive the famed 't Hooft interaction on the light front. In Sec. IX we use our light-front wave functions to derive the parton distributions functions and amplitudes of heavy and light mesons, and their pertinent low energy constants. The extraction of the mesonic form factors is also briefly discussed. Our conclusions are in Sec. X. A number of appendices are added to complement some of the results in the text.

II. PERTURBATIVE LIGHT-FRONT HAMILTONIAN, VIA ANALYTIC CONTINUATION FROM EUCLIDEAN AMPLITUDES

In the infinite momentum frame, a meson state composed of a quark and antiquark $Q\bar{Q} \equiv Q_1 Q_2$ is characterized by the closed Wilson loop or a *dipole*, sloped along the light cone with rapidity χ as shown in Fig. 1. The same Wilson loop follows from the Euclidean Wilson loop at an angle θ by analytical continuation $\theta \rightarrow -i\chi$, as we discussed in Paper II of this series [17]. This construction follows the original suggestion for quark-quark scattering in [20], and its extension to *dipole-dipole* scattering in the QCD vacuum [21,22], many years ago. The same construction was used in the holographic context, to address hadron-hadron scattering in the Regge limit [23–25].

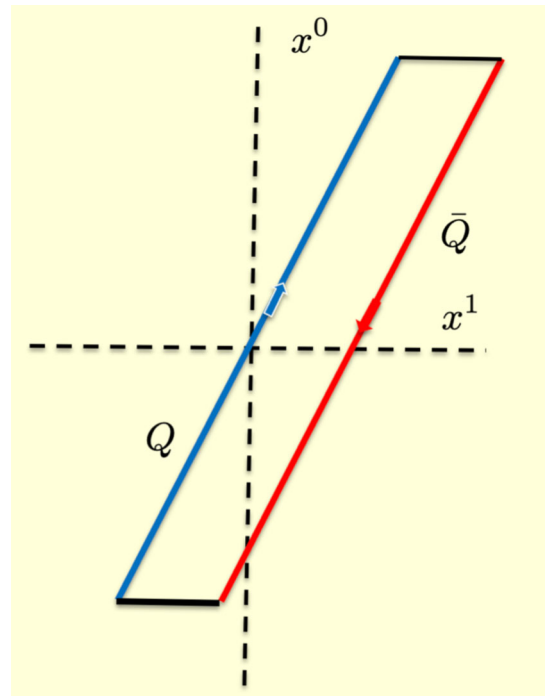


FIG. 1. Wilson loop for a $\bar{Q}Q$ meson on the light front.

With this in mind, the result is the squared meson mass operator, or light-front Hamiltonian H_{LF}

$$\begin{aligned} H_{LF} &\approx \frac{k_{\perp}^2 + m_Q^2}{x\bar{x}} + 2P^+P^- \\ &\approx \frac{k_{\perp}^2 + m_Q^2}{x\bar{x}} + 2M(\mathbb{V}_{Cg}(\xi_x) + \mathbb{V}_C(\xi_x) \\ &\quad + \mathbb{V}_{SD}(\xi_x, b_{\perp}) + \mathbb{V}_{TH}(\xi_x, b_{\perp})). \end{aligned} \quad (1)$$

The nonperturbative contributions in (1) were discussed in [17], along with the ordering ambiguities. The perturbative contributions will be derived below. On the light front, the invariant distance ξ_x is

$$\xi_x = \left(\left| \frac{id/dx}{M} \right|^2 + b_{\perp}^2 \right)^{\frac{1}{2}} \quad (2)$$

with longitudinal distance $\gamma b_3 = id/dx/M$, the conjugate of Bjorken x or $x = k^3/P^3$. The explicit γ -factor compensates the Lorentz contraction along the 3-direction.

The Hamiltonian (1) is gauge invariant. The free kinetic part stems from the free quark propagators associated to the massive quarks tracing the Wilson loop in Fig. 1, with no explicit gauge fields. The gauge fields are implicit in the formation of the constituent quark mass, through the spontaneous breaking of chiral symmetry with a finite m_Q , which we are assuming. The explicit coupling of the Wilson lines to the external gauge fields in Fig. 1 is what gives rise to $2P^+P^-$ as we detail below.

A. Wilson lines dressed by spin variables

The perturbative contribution to the central potential on the light front, induced by a one-gluon exchange with an effective mass m_G in the random instanton vacuum (RIV), can be constructed using the general technique of a sloped Wilson loop as we detailed in [17]. In particular, the one-gluon interaction with spin effects follows by dressing the Wilson loop or holonomies in Fig. 1, with explicit spin factors

$$\begin{aligned} &\left\langle \text{Tr} \left[\mathbf{P} \exp \left(+g \int d\tau_1 (i\dot{x}(\tau_1) \cdot A(x(\tau_1)) + \frac{1}{4} \sigma_{1\mu\nu} F_{\mu\nu}(x(\tau_1))) \right) \right. \right. \\ &\quad \left. \left. \times \mathbf{P} \exp \left(+g \int d\tau_2 (i\dot{x}(\tau_2) \cdot A(x(\tau_2)) + \frac{1}{4} \sigma_{2\mu\nu} F_{\mu\nu}(x(\tau_2))) \right) \right] \right\rangle \end{aligned} \quad (3)$$

with $\sigma_{\mu\nu} = \frac{1}{2i}[\gamma_{\mu}, \gamma_{\nu}]$ and $\sigma_{\mu\nu} = \eta_{a\mu\nu}\sigma^a$ using the 't Hooft symbol. The averaging is understood using the QCD action. We have made explicit the gauge coupling g , for a perturbative treatment to follow.

For massive quarks travelling on straight trajectories, the affine time τ relates to the conventional time t through

$$\mu = \frac{dt}{d\tau} = \frac{m_Q}{\sqrt{1 + \frac{\dot{x}^2}{x^2}}} \rightarrow \gamma m_Q \quad (4)$$

in Euclidean signature. We note that the holonomies tracing out the Wilson loop in Fig. 1 are unaffected by the exchange $\tau \rightarrow t$, in contrast to the spin contributions which get rescaled by $1/\mu$. This will be exploited below.

B. One-gluon exchange and the Coulomb interaction

The Coulomb interaction between a $Q\bar{Q} \equiv Q_1Q_2$ pair attached to the Wilson lines can be obtained in perturbation theory by expanding the holonomies and averaging the AA correlator in leading order. For that, we parametrize the worldlines by

$$\begin{aligned} x_{\mu}(t_1) &= (0, 0, \sin \theta t_1, \cos \theta t_1), \\ x_{\mu}(t_2) &= (b_1, b_2, \sin \theta t_2 + b_3, \cos \theta t_2). \end{aligned} \quad (5)$$

The perturbative one-gluon contribution from (3) reads

$$g^2 T_1^A T_2^B \int dt_1 \int dt_2 (\cos^2 \theta \langle A_4^A(t_1) A_4^B(t_2) \rangle + \sin^2 \theta \langle A_3^A(t_1) A_3^B(t_2) \rangle + 2 \sin \theta \cos \theta \langle A_4^A(t_1) A_3^B(t_2) \rangle) \quad (6)$$

with the gluon correlator in Feynman gauge

$$\langle A_{\mu}^A(t_1) A_{\nu}^B(t_2) \rangle = \frac{1}{2\pi^2} \frac{\delta^{AB} \delta_{\mu\nu}}{|x(t_1) - x(t_2)|^2}. \quad (7)$$

Inserting (7) into (6) and changing variables $T_E = t_1 + t_2$ and $\tau = t_1 - t_2$ yields

$$\begin{aligned} &\frac{g^2 T_1^A T_2^A}{2\pi^2} \int \frac{dT_E}{2} \int dt \frac{1}{t^2 + \cos^2 \theta b_3^2 + b_{\perp}^2} \\ &= \frac{g^2 T_1^A T_2^A}{4\pi} \frac{T_E}{\sqrt{b_3^2 \cos^2 \theta + b_{\perp}^2}}. \end{aligned} \quad (8)$$

The analytical continuation $\theta \rightarrow -i\chi$ and $T_E \rightarrow iT_M$ of (8) reexponentiates to the Coulomb contribution

$$\exp\left[-i\gamma T_M\left(-\frac{g^2 T_1^A T_2^A}{4\pi}\frac{1/\gamma}{\sqrt{\gamma^2 b_3^2 + b_\perp^2}}\right)\right] \quad (9)$$

with γT_M the dilatated time along the lightlike Wilson loop. The Coulomb contribution to the light-front $Q\bar{Q}$ Hamiltonian P_{Cg}^- follows, leading the squared invariant mass as

$$\begin{aligned} 2P^+ P_{Cg}^- &= 2P^+\left(-\frac{g^2 T_1^A T_2^A}{4\pi}\frac{1/\gamma}{\sqrt{\gamma^2 b_3^2 + b_\perp^2}}\right) \\ &\rightarrow 2M\left(-\frac{g^2 T_1^A T_2^A}{4\pi}\frac{1}{\xi_x}\right) = 2M\mathbb{V}_{Cg}(\xi_x) \end{aligned} \quad (10)$$

with $P^+/M = \gamma$, and $\gamma b_3 \rightarrow id/dx/M$ the conjugate of Bjorken x .

In the RIV, the perturbative gluons acquire a momentum dependent mass from their rescattering through the instanton–anti-instanton ensemble [26]

$$\begin{aligned} m_G(k\rho) &= m_G(k\rho K_1(k\rho)), \\ m_{G\rho} &\approx 2\left(\frac{6\kappa}{N_c^2 - 1}\right)^{\frac{1}{2}} \approx 0.55 \end{aligned} \quad (11)$$

using the estimate $\kappa = \pi^2 \rho^4 n_{I+\bar{I}}$ in the right-most result. With this in mind, (10) is now

$$\mathbb{V}_{Cg}(\xi_x) = -\frac{g^2 T_1^A T_2^A}{2\pi^2} \frac{1}{\xi_x} \int_0^\infty \frac{dx x \sin x}{x^2 + (\xi_x m_G(x\rho/\xi_x))^2} \rightarrow -\frac{g^2 T_1^A T_2^A}{4\pi} \frac{e^{-m_G \xi_x}}{\xi_x} \quad (12)$$

with the right-most result following for a constant gluon mass.

C. Spin-spin interaction

The perturbative spin-spin interaction follows from the cross term in (3)

$$-\frac{g^2}{16} \int d\tau_1 d\tau_2 \langle \sigma_{1\mu\nu} F_{\mu\nu}(x(\tau_1)) \sigma_{2\alpha\beta} F_{\alpha\beta}(x(\tau_2)) \rangle. \quad (13)$$

Note that the perturbative electric field is purely imaginary in Euclidean signature, leading mostly to phases and not potentials in the long time limit. Also, the Dirac representation σ_{4i} is off-diagonal, an indication that the electric contribution mixes particles and antiparticles, which is excluded by the use of straight Wilson lines on the light front. With this in mind and using (4), we can reduce (13) to

$$\begin{aligned} &-\frac{g^2}{4\mu^2} \int dt_1 dt_2 \langle \sigma_{1ij} F_{ij}(x(t_1)) \sigma_{2kl} F_{kl}(x(t_2)) \rangle \\ &= -\frac{g^2}{4\mu^2} \sigma_1^a \sigma_2^b \int dt_1 dt_2 \langle B_a(x(t_1)) B_b(x(t_2)) \rangle \end{aligned} \quad (14)$$

with

$$\begin{aligned} &\langle B_a(x(t_1)) B_b(x(t_2)) \rangle \\ &= T_1^A T_2^B \epsilon_{aij} \epsilon_{bkl} \partial_{1i} \partial_{2k} \langle A_j^A(x(t_1)) A_m^B(x(t_2)) \rangle \\ &= T_1^A T_2^A (\delta_{ab} \delta_{ik} - \delta_{ak} \delta_{bi}) \partial_{1i} \partial_{2k} \\ &\quad \times \frac{1}{2\pi^2} \frac{1}{|x(t_1) - x(t_2)|^2}. \end{aligned} \quad (15)$$

Inserting (15) into (14), and carrying the time integrations along the sloped Wilson loop in Fig. 1 gives among others

$$-\frac{g^2 T_1^A T_2^A}{4\pi} \frac{T_E}{4\mu^2} \left[\sigma_{1\perp} \cdot \sigma_{2\perp} \left(-3 \cos^2 \theta \frac{(\cos \theta b_3)^2}{\xi_\theta^2} + \cos^2 \theta \right) \frac{1}{\xi_\theta^3} \right] \quad (16)$$

which is the dominant contribution under the analytical continuation $\theta \rightarrow -i\chi$, $\mu \rightarrow \gamma m_Q$ and $T_E \rightarrow iT_M$, in the ultrarelativistic limit $\gamma \gg 1$, and in Minkowski signature. The final spin-spin contribution to the squared mass is in general

$$\begin{aligned} H_{SS} &= 2M \left[\frac{\sigma_{1\perp} \cdot \sigma_{2\perp}}{4m_{Q1} m_{Q2}} (\nabla_\perp^2 \mathbb{V}_{Cg}(\xi_x)) \right] \\ &= 2M \mathbb{V}_{SS}(\xi_x, b_\perp). \end{aligned} \quad (17)$$

D. Spin-orbit interaction

1. Cross spin orbit

The cross spin-orbit interaction is readily obtained from the 12 + 21 cross terms

$$\begin{aligned} &-\frac{g^2 T_1^A T_2^B}{2} \sigma_2^a \int d\tau_1 d\tau_2 i \dot{x}_i(\tau_1) \langle A_i^A(x(\tau_1)) B_a^B(x(\tau_2)) \rangle \\ &\quad + 1 \leftrightarrow 2 \end{aligned} \quad (18)$$

which can be reduced to

$$\begin{aligned} &-\frac{ig^2 T_1^A T_2^B \sin \theta}{2\mu} \sigma_2^a s_1 \int dt_1 dt_2 \langle A_i^A(x(t_1)) B_a^B(x(t_2)) \rangle \\ &\quad + 1 \leftrightarrow 2 \end{aligned} \quad (19)$$

with $s_{1,2} = \text{sgn}(v_{1,2}^3)$ the signum of the 3-velocity of particle 1,2 (a more refined definition will be given below). After carrying the integrations, and the analytical continuations, the spin-orbit contribution to the squared mass is

$$H_{SL,12} = 2M \left[\left(\frac{\sigma_2 \cdot (b_{12} \times s_1 \hat{3})}{2m_{Q2}} - \frac{\sigma_1 \cdot (b_{21} \times s_2 \hat{3})}{2m_{Q1}} \right) \left(\frac{1}{\xi_x} \mathbb{V}'_{Cg}(\xi_x) \right) \right] \quad (20)$$

in general, with $b_{21} = -b_{12} \equiv b_\perp$.

2. Standard spin orbit

The standard self-spin-orbit interaction with Thomas precession is more subtle. To unravel it, we note that the insertion of a single spin contribution along the path-ordered Wilson loop amounts to expanding the spin factors in (3) to first order, and retaining the holonomies to all orders in $\mathbf{1}_\theta$, namely,

$$\frac{1}{4\mu} \sigma_{1\mu\nu} \int dt_1 \langle gF_{\mu\nu}(x(t_1)) \mathbf{1}_\theta \rangle + 1 \leftrightarrow 2 \quad (21)$$

with the path ordered color-spin trace subsumed. Here $\mathbf{1}_\theta$ refers to the slated Wilson loop in Fig. 1 without the spin dressing. We now decompose

$$F_{\mu\nu} = v_{1\mu} v_{1\alpha} F_{\alpha\nu} + F_{\mu\nu}^\perp \equiv F_{\mu\nu}^\parallel + F_{\mu\nu}^\perp \quad (22)$$

into a contribution parallel to $v_1 = \dot{x}_1$ and a contribution orthogonal to v_1 . The contribution parallel to the worldline when inserted in (21) can be undone by the identity (see Eq. (71) in [17])

$$\int dt_1 \langle gv_\alpha F_{\alpha\nu}(x(t_1)) \mathbf{1}_\theta \rangle = -i\partial_{1\nu} \langle \mathbf{1}_\theta \rangle \equiv -i\partial_{1\nu} e^{-T_E \mathbb{V}_C(\xi_\theta)} \quad (23)$$

with $\mathbb{V}_C(\xi_\theta) \approx \mathbb{V}_{Cg}(\xi_\theta)$ the central Coulomb potential in perturbation theory. The longitudinal contribution to (21)

$$-\frac{1}{4\mu} \sigma_{1\mu\nu} v_{1\mu} i\partial_{1\nu} e^{-T_E \mathbb{V}_C(\xi_\theta)} + 1 \leftrightarrow 2 \quad (24)$$

is gauge invariant. After carrying the analytical continuation, (24) contributes both a real and imaginary part. The latter is an irrelevant phase factor in Euclidean signature. The *real* part contributes to the direct mass squared operator as

$$H_{LS,11} = 2M \left[\left(\frac{\sigma_1 \cdot (b_{12} \times s_1 \hat{3})}{4m_{Q1}} - \frac{\sigma_2 \cdot (b_{21} \times s_2 \hat{3})}{4m_{Q2}} \right) \left(\frac{1}{\xi_x} \mathbb{V}'_{Cg}(\xi_x) \right) \right] \quad (25)$$

in leading order in perturbation theory. This is the standard spin-orbit contribution with the correct Thomson correction on the light front, familiar from atomic physics in the rest frame. The total perturbative spin contribution on the light front is the sum of (17), (20), and (25),

$$H_{LS,g} = 2M \left(\frac{l_{1\perp} \cdot S_{1\perp}}{2m_{Q1}^2} - \frac{l_{2\perp} \cdot S_{2\perp}}{2m_{Q2}^2} + \frac{l_{1\perp} \cdot S_{2\perp}}{m_{Q1}m_{Q2}} - \frac{l_{2\perp} \cdot S_{1\perp}}{m_{Q1}m_{Q2}} \right) \frac{1}{\xi_x} \mathbb{V}'_{Cg}(\xi_x) + 2M \left(\frac{S_{1\perp} \cdot S_{2\perp}}{m_{Q1}m_{Q2}} \right) \nabla_\perp^2 \mathbb{V}_{Cg}(\xi_x) \quad (26)$$

with the respective spins $\vec{S}_{1,2} = \vec{\sigma}_{1,2}/2$, and transverse orbital momenta

$$l_{1,2\perp} = \pm (b_\perp \times m_{Q1,2} s_{1,2} \hat{3})_\perp, \quad s_{1,2} = \text{sgn}(v_{1,2}) \rightarrow \frac{Mx_{1,2}}{m_{Q1,2}}. \quad (27)$$

III. INSTANTON CONTRIBUTIONS TO WILSON LINE AMPLITUDES

A. Central potential

The central potential operator induced by instantons is given by

$$\mathbb{V}_C(\xi_x) = \left(\frac{4\kappa}{N_c \rho} \right) \mathbf{H}(\tilde{\xi}_x) \quad (28)$$

with the integral operator

$$\begin{aligned} \mathbf{H}(\xi_x) = & \int_0^\infty y^2 dy \int_{-1}^{+1} dt \left[1 - \cos\left(\frac{\pi y}{\sqrt{y^2 + 1}} \right) \cos\left(\pi \left(\frac{y^2 + \tilde{\xi}_x^2 + 2\tilde{\xi}_x y t}{y^2 + \tilde{\xi}_x^2 + 2\tilde{\xi}_x y t + 1} \right)^{\frac{1}{2}} \right) \right. \\ & \left. - \frac{y + \tilde{\xi}_x t}{(y^2 + \tilde{\xi}_x^2 + 2\tilde{\xi}_x y t)^{\frac{1}{2}}} \sin\left(\frac{\pi y}{\sqrt{y^2 + 1}} \right) \sin\left(\pi \left(\frac{y^2 + \tilde{\xi}_x^2 + 2\tilde{\xi}_x y t}{y^2 + \tilde{\xi}_x^2 + 2\tilde{\xi}_x y t + 1} \right)^{\frac{1}{2}} \right) \right] \end{aligned} \quad (29)$$

with the dimensionless invariant distance on the light front $\tilde{\xi}_x = \xi_x/\rho$. $\mathbf{H}(\tilde{\xi}_x)$ admits the short distance limit

$$\mathbf{H}(\tilde{\xi}_x) \approx + \left(\frac{\pi^3}{48} - \frac{\pi^3}{3} J_1(2\pi) \right) \tilde{\xi}_x^2 + \left(-\frac{\pi^3(438 + 7\pi^2)}{30720} + \frac{J_2(2\pi)}{80} \right) \tilde{\xi}_x^4 \quad (30)$$

and large distance limit

$$\mathbf{H}(\xi_x) \approx -\frac{2\pi^2}{3} (\pi J_0(\pi) + J_1(\pi)) + \frac{C}{\xi_x^p} \quad (31)$$

with $p \ll 1$ and $C > 0$. The large asymptotic is to be subtracted in the definition of the potential. This will be subsumed throughout. In the dense instanton vacuum discussed in [17], the central potential (28) is almost linear at intermediate distances 0.2–0.5 fm. At larger distances, the linearly confining potential with string tension σ_T takes over, in good agreement with most lattice simulations.

B. Spin-dependent potentials

On the light front, the spin-dependent interactions captured by V_{SD} and due to the nonzero modes in (1) have been discussed in general in [17], with the results

$$\begin{aligned} \mathbb{V}_{SD}(\xi_x, b_\perp) = & + \left[\frac{\sigma_1 \cdot (b_{12} \times s_1 \hat{3})}{4m_{Q1}} - \frac{\sigma_2 \cdot (b_{21} \times s_2 \hat{3})}{4m_{Q2}} \right] \frac{1}{\xi_x} \mathbb{V}'_C(\xi_x) \\ & + \left[\frac{\sigma_1 \cdot (b_{12} \times s_1 \hat{3})}{2m_{Q1}} - \frac{\sigma_2 \cdot (b_{21} \times s_2 \hat{3})}{2m_{Q2}} \right] \frac{1}{\xi_x} \mathbb{V}'_1(\xi_x) \\ & + \left[\frac{\sigma_2 \cdot (b_{12} \times s_1 \hat{3})}{2m_{Q2}} - \frac{\sigma_1 \cdot (b_{21} \times s_2 \hat{3})}{2m_{Q1}} \right] \frac{1}{\xi_x} \mathbb{V}'_2(\xi_x) \\ & + \left[\frac{1}{4m_{Q1}m_{Q2}} \left[\left(\sigma_{1\perp} \cdot \hat{b}_{21} \sigma_{2\perp} \cdot \hat{b}_{21} - \frac{1}{2} \sigma_{1\perp} \cdot \sigma_{2\perp} \right) \right] \right] \mathbb{V}_3(\xi_x) \end{aligned} \quad (32)$$

with again $b_{21} = -b_{12} \equiv b_\perp$. All potentials follow from the central instanton potential $\mathbb{V}_C(\xi_x)$, thanks to self-duality

$$\begin{aligned} \mathbb{V}_1(\xi_x) &= \mathbb{V}_2(\xi_x) - \mathbb{V}_C(\xi_x) = -\frac{1}{2} \mathbb{V}_C(\xi_x), \\ \mathbb{V}_2(\xi_x) &= +\frac{1}{2} \mathbb{V}_C(\xi_x), \\ \mathbb{V}_3(\xi_x) &= +2 \frac{b_\perp^2}{\xi_x^2} \mathbb{V}''_C(\xi_x). \end{aligned} \quad (33)$$

As a result, the first and second contribution in (32) cancel out, leaving only the cross spin orbit plus tensor contributions in the instanton vacuum,

$$H_{LS} = 2M \left(\left(\frac{l_{1\perp} \cdot S_{2\perp}}{m_{Q1}m_{Q2}} - \frac{l_{2\perp} \cdot S_{1\perp}}{m_{Q1}m_{Q2}} \right) \frac{1}{\xi_x} \mathbb{V}'_C(\xi_x) + \frac{1}{m_{Q1}m_{Q2}} \left(S_{1\perp} \cdot \hat{b}_\perp S_{2\perp} \hat{b}_\perp - \frac{1}{2} S_{1\perp} \cdot S_{2\perp} \right) \frac{2b_\perp^2}{\xi_x} \mathbb{V}''_C(\xi_x) \right) \quad (34)$$

with $\vec{l}_{1,2}$ given in (27), and $V_C(\xi_x)$ in (28). The contributions stemming from the zero modes are not included. They will be discussed separately below.

IV. HEAVY QUARKONIA ON THE LIGHT FRONT

In Paper II [17] we introduced “the basic problem” of meson structure, of two constituent quarks connected by a classical relativistic string, which was then studied using

both a semiclassical approach, and a relativistic Klein-Gordon equation. Our main focus there was on the correspondence between the conventional treatment in the rest frame versus the analysis on the light front using the Hamiltonian we derived. Of course, frame-invariant quantities—masses in particular—obtained in both ways must agree. We specifically investigated the linear rise of the Regge trajectories, with the principal quantum number $M_n^2 \sim n$ (not angular momentum).

In this paper we will carry out a larger set of studies, including not only the confining string, but also various other terms in the Hamiltonian. In particular, the perturbative (Coulomb) term, and most importantly, the terms containing spin and orbital momentum variables. In doing so, it is also natural to widen the set of applications. Therefore here we start with heavy quarkonia, before returning to the light quark systems.

In the quarkonia settings, we can use the large quark mass as an extra parameter, to discriminate between distinct physical contributions. Remarkably, on the light front all meson problems, from bottomonia to pions, can be studied in essentially the same setting, just by changing the mass value.

A. Excited states of bottomonium via the Schrödinger equation in the rest frame

Let us start by focusing first on heavy quarkonia. Such an approach is more convenient in this work, devoted to the mixing between states with different spin and orbital momenta. In heavy quarkonia these relativistic effects are naturally suppressed by the nonrelativistic motion of heavy quarks (or, in other terms, their small magnetic moments $\mu \sim g/m_Q$).

The first question to be addressed is, how well can the heavy quarkonia states be represented by linear-linear Regge trajectories? In Fig. 2 we show the experimental masses of the (nS), $n = 0-5$ Upsilon's, compared to the standard results from the Schrödinger equation, with the Cornell potential (black triangles) and with only its linear part $V_{\text{conf}} = \sigma_T r$ (blue circles). The first observation is that

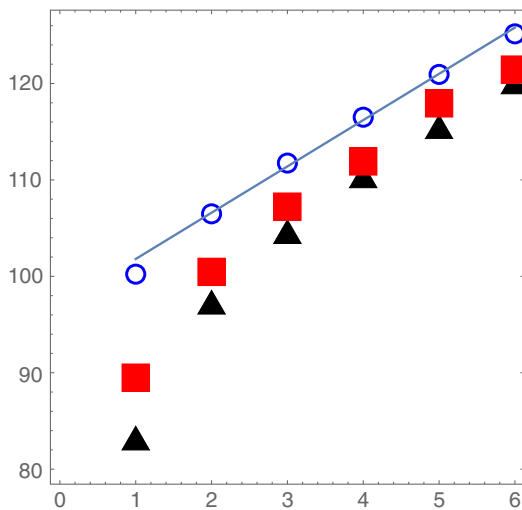


FIG. 2. M_{n+1}^2 (GeV)² versus $n + 1$, $n = 0, \dots, 5$, for the six S zero orbital momentum ($L = 0$) states of bottomonium. The red squares correspond to the experimentally observed Upsilon's. The black triangles show the masses obtained from the Schrödinger equation, with the Cornell potential (linear and Coulomb potentials, no spin forces). The blue circles show the masses if the Coulomb potential is switched off, and only the linear potential is used. The straight line is shown for comparison.

by using a linear potential alone (blue circles), we find a nearly linear Regge trajectory. This observation will be important in the next subsection, as it shows that even for heavy bottomonia, the light-front Hamiltonian can be approximated by an oscillator with good accuracy. Note however, that the slope of the straight line is here completely different from the $1/\alpha'$ slope of a similar trajectory for light mesons (e.g. for ω mesons we used in [16]).

The second observation is that the expected contribution from the spin-dependent potential V_{SS} (responsible for splitting between squares and triangles) is positive and decreases with n . The former is due to the positivity of the spin factor $\vec{S}_1 \cdot \vec{S}_2 = 1/4$, and the second to the fact that $V_{SS}(r)$ is rather short range, in comparison to the size of the lowest Upsilon, but much smaller than the sizes of the excited ones. Another way to anticipate the accuracy of an oscillator approximation in the light-front description (discussed in [17] and using ω_3 mesons with $L = 2$) is to study the mass dependence of bottomonium on its orbital momentum L . In Fig. 3 we show the calculated 18 squared masses for $n = 0-5$ (left to right) and $L = 0, 1, 2$ (bottom to top). While the Coulomb potential was included, it affects mostly and only $n = 0, L = 0$ Upsilon. The Regge trajectories for nonzero angular momentum $L = 1, 2$ show better linear dependence on n than $L = 0$. The corresponding wave function vanishes at the origin $r = 0$, and is less affected by short-range Coulomb and spin-dependent forces.

We further note, that at larger n (right side of the plot) the dependence on L also becomes linear, as the $L = 0, 1, 2$ points become equidistant. This observation encourages us to think that the oscillator description of the light-front

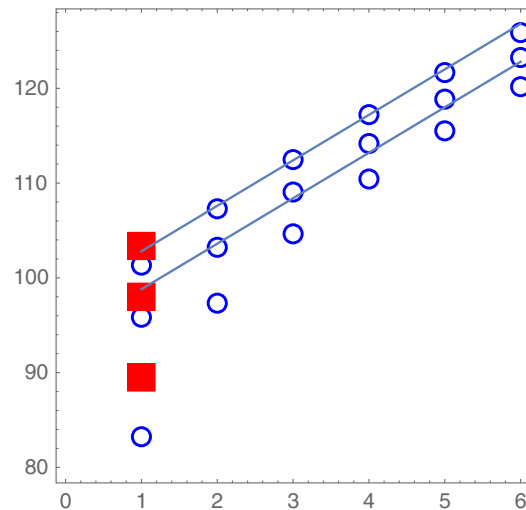


FIG. 3. M_{n+1}^2 (GeV)² versus $n + 1$, $n = 0, 1, \dots$ for three families of bottomonium states, with orbital momentum $L = 0, 1, 2$ (from bottom up). The red squares correspond to the experimentally observed $\Upsilon, h_b, \Upsilon_2$ mesons (from bottom up). The blue circles show masses obtained from the Schrödinger equation, with the Cornell potential (linear and Coulomb potentials, still without spin forces). The straight lines are shown for comparison.

Hamiltonian and light-front wave functions (LFWFs), will need only relatively small corrections.

B. Bottomonium on the light front

In [17], we described how we may include the linear confining term in H_{LF} (instanton induced at intermediate distances), and make it more user friendly, by eliminating the square root using the well-known einbein $e = 1/a$ trick, i.e.

$$2M\mathbb{V}_C(a, b, x, b_\perp) \approx \sigma_T \left(\frac{|id/dx|^2 + bb_\perp^2}{a} + a \right). \quad (35)$$

Here a, b are variational parameters. The minimization with respect to a is assumed, followed by the substitution $b \rightarrow M^2 \approx (2m_Q)^2$ for heavy mesons, and most light ones. (For the pion, this last substitution is not valid, as we have shown in [17].)

For a numerical analysis of (35), we used in [17] a basis set of functions composed of a two-dimensional transverse oscillator times longitudinal states $\sin(\pi n x)$ with odd n , as we briefly review in Appendix A. More specifically, the light-front Hamiltonian can be rearranged as follows,

$$H_{LF} = H_0 + \tilde{V} + V_{\text{perp}} + V_{\text{spin}} \quad (36)$$

with the spin part including both the perturbative and nonperturbative instanton contributions. As we noted earlier, in the dense instanton vacuum, the central part is hardly differentiable from the linear confining potential at intermediate distances.

The first contribution H_0

$$H_0 = \frac{\sigma_T}{a} \left(-\frac{\partial^2}{\partial x^2} - b \frac{\partial^2}{\partial k_\perp^2} \right) + \sigma_T a + 4(m_Q^2 + k_\perp^2) \quad (37)$$

is diagonal in the functional basis used [17]. In this form, we make use of the momentum representation, with \vec{k}_\perp as variable. Similarly, one can use the coordinate representation with \vec{b}_\perp as a variable, and $\vec{k}_\perp = i\partial/\partial\vec{b}_\perp$. The latter choice is much more convenient when discussing states with nonzero angular momenta, in relation to the azimuthal angle coordinate ϕ in the transverse plane (see more on that in Appendix E).

The second contribution \tilde{V}

$$\tilde{V}(x, \vec{k}_\perp) \equiv (m_Q^2 + k_\perp^2) \left(\frac{1}{x\bar{x}} - 4 \right) \quad (38)$$

has nonzero matrix elements $\langle n_1 | V(x, \vec{k}_\perp) | n_2 \rangle$ for all n_1, n_2 pairs. The perturbative part V_{perp} for heavy quarks is the Coulomb term, with running coupling and other radiative corrections. Finally, the last term V_{spin} contains matrices in spin variables and in orbital momenta, which we will consider later.

We truncate the basis set to a 12×12 matrix, and diagonalize $H_0 + \tilde{V}$ to find its eigenvalues as a function

of the remaining parameter a . The results for the three lowest states $n = 1, 2, 3$ are shown in Fig. 4 (top). We see that while the minima in a exist, they are not at the same value. Thus the dilemma: one can either select different a for different states, and then somehow reorthogonalize them, or one can use some ‘‘optimal’’ value of a common for all states, and then be sure that all states are orthogonal. Since the dependence on a is rather flat, we opt for the second approach and use $a = 25$.

The calculated masses (shifted by a constant ‘‘mass renormalization’’ to make $n = 0, m = 0$ states the same) are shown in Fig. 4. The bottom part shows good agreement between the masses obtained solving the Schrödinger equation in the rest frame (blue circles), and the masses following from the light-front frame (red triangles). The slope is correct, and is determined by the same string tension σ_T . The splittings in orbital momentum are of the same scale, but not identical. This is expected, as we compare the

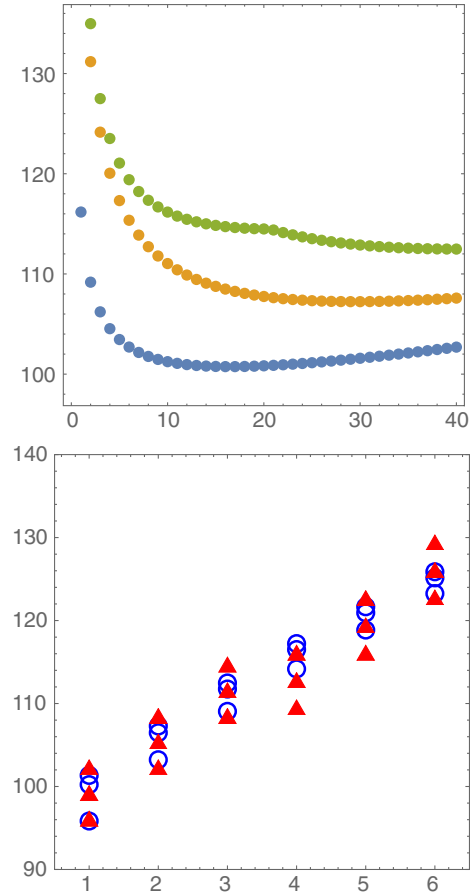


FIG. 4. Top: squared masses M_n^2 for $\bar{b}b$ mesons for $n = 1, 2, 3$ versus the variational parameter a . Bottom: squared masses for $n = 0.5$ (left to right) and orbital momentum $m = 0, 1, 2$ (down to up), calculated from the light-front Hamiltonian H_{LF} (red triangles), and shifted by a constant, $M_{n+1}^2 - 5 \text{ GeV}^2$. For comparison, the blue circles show the squared masses M_{n+1}^2 calculated from Schrodinger equation in the CM frame, with only linear plus centrifugal potentials.

two-dimensional m states on the light front, with the three-dimensional L states in the center-of-mass frame.

The irregularity between the third and fourth sets of states is due to our use of a modest basis set, with only three radial functions (altogether 12 functions if one counts them with 4 longitudinal harmonics). This can be eliminated using a larger set.

As a final note in this section, we recall that the chief goal of these calculations is to generate the pertinent LFWFs for all of these states, from the light-front Hamiltonian H_{LF} . The details about the setting and some of these wave functions can be found in Appendices A–C.

C. Matrix elements of the Coulomb term and further operators on the LF

We start with a calculation of the contribution of the Coulomb force, which demonstrates how to deal with any function of transverse coordinate $F(r_\perp)$, with $r_\perp = b_\perp$. Of course, the standard way is to transform all functions into the coordinate representation.

Recall that our LFWFs are defined using a transverse oscillator in the *momentum representation*, and so one possible strategy is to trade

$$\vec{r}_\perp \rightarrow i \frac{\partial}{\partial \vec{k}_\perp}$$

as in the confining potential. It can work for other polynomial functions $F(r_\perp)$ or their Taylor expansions. Unfortunately, for a transverse Coulomb potential

$$V_\perp = -\frac{C_C}{r_\perp} \quad (39)$$

this strategy does not work. A straightforward solution is to Fourier transform the LFWFs to coordinate representation. Note that the LFWFs are of the form

$$\psi(p_\perp, x) = \sum_n \phi_n(p_\perp) \sin(\pi n x).$$

The same procedure applies for the excited states. Equation (44) shows the natural transverse cutoff in $b_\perp \sim \pi/M \sim \pi/2m_Q$ for the heavy states.

V. SPIN AND ORBITAL MOMENTUM MIXING OF THE LFWFs

So far, we have only discussed the LFWFs diagonal in longitudinal orbital momentum $L_z = m$. In general, this is not a conserved quantity, but for heavy quarkonia it is

As a result, the integration over x in the matrix element $\langle \psi | F(r_\perp) | \psi \rangle$ removes terms with $n_1 \neq n_2$, and reduces to

$$\langle \psi | F(r_\perp) | \psi \rangle = \sum_n \int d^2 r_\perp |\tilde{\phi}_n(r_\perp)|^2 F(r_\perp) \quad (40)$$

where tilde stands for the Fourier transform.

In particular, the lowest state in our basis has a simple Gaussian form $\phi_1(p_\perp) \sim \exp(-Ap_\perp^2)$, and its Fourier transform is also a Gaussian $\tilde{\phi}_1(r_\perp) \sim \exp(-\frac{r_\perp^2}{4A})$. The average Coulomb contribution to the squared mass M_Υ^2 is then found to be

$$-4M_b \langle \psi_1 | \frac{C_C}{r_\perp} | \psi_1 \rangle = -4M_b C_C \sqrt{\frac{\pi}{2A}} \approx -15 \text{ GeV}^2 \quad (41)$$

which approximately agrees with $\Delta M_\Upsilon^2 \approx -17 \text{ GeV}^2$ obtained from the Schrödinger equation in the CM frame (and shown in Fig. 2). With growing Upsilon number their sizes grow, which reduces the Coulomb contribution.

In general, the operators to be averaged (e.g. spin-dependent potentials) depend on the invariant distance ξ_x , which includes the longitudinal distance with the derivative id/dx . In this case the matrix element should be calculated using the eigenvalue l decomposition of this derivative operator. For example, by approximating the ground state LFWF as

$$\phi_0(x, p_\perp) \approx \left(\frac{2\alpha}{\pi}\right)^{\frac{1}{2}} e^{-\alpha p_\perp^2/2} \sum_{\text{odd}l} \varphi_l \sin(l\pi x) \quad (42)$$

with a simple Fourier transform $p_\perp \rightarrow b_\perp$

$$\tilde{\phi}_0(x, b_\perp) \approx \left(\frac{2}{\pi\alpha}\right)^{\frac{1}{2}} e^{-b_\perp^2/2\alpha} \sum_{\text{odd}l} \varphi_l \sin(l\pi x) \quad (43)$$

one can use it to evaluate matrix elements of a potential depending on this invariant $V(\xi)$ as follows:

$$\langle \phi_0 | V(\xi_x) | \phi_0 \rangle = \int db_\perp \frac{e^{-b_\perp^2/\alpha}}{\pi\alpha} \sum_{\text{odd}l} |\varphi_l|^2 V\left(\left(\left(\frac{l\pi}{M\rho}\right)^2 + \frac{b_\perp^2}{\rho^2}\right)^{\frac{1}{2}}\right). \quad (44)$$

approximately conserved, as the spin and orbital momentum-dependent effects are suppressed by large quark masses. As we will proceed to light quark states, this approach would become invalid, and spin-spin and spin-orbit mixing is mandatory.

A. Parity on the light front

There are some obvious differences between the description in the rest frame, and on the light front. For instance, there are different symmetries: three-dimensional angular

momenta \vec{S} , \vec{L} , \vec{J} are reduced to their two-dimensional transverse parts, with spin \vec{S} and orbital momentum \vec{L} projected onto longitudinal momentum \vec{P} . The projection of J is denoted by “meson helicity” Λ . Obviously, hadron states with different Λ values, are treated differently: say $\rho(\Lambda = 0)$ and $\rho(\Lambda = \pm 1)$ have different wave functions (even more than one: see below). While masses, magnetic and quadrupole moments, etc. should turn out to be the same, the three-dimensional rotation is some complicated transformation, involving all components of the wave functions, and we will not attempt to explicitly use it.

(This situation is of course not new. For example, different isospin components are also treated differently in the rest frame. The $\bar{d}u$ charged states are described by a potential, while the $\bar{d}d$, $\bar{u}u$ follow from annihilation. In the isospin symmetric limit, the same mass for π^+ and π^0 needs to be explicitly demonstrated.)

Another important difference between the rest frame and the light-front frame notations relates to the different definitions of parity. The usual P -parity is the sign change of *all* three spatial coordinates, or mirror reflection. On the light front, one would like to keep the main beam direction (of \vec{P}) intact, so P is supplemented by an additional rotation, by π around some transverse axes: this operator is called \hat{Y} . The state’s helicity Λ changes sign, so its action for $\Lambda \neq 0$ is given by the so-called Jacob-Wick relation

$$\hat{Y}|\vec{P}, \Lambda\rangle = (-)^{S-\Lambda}\eta|\vec{P}, -\Lambda\rangle, \quad (45)$$

where η is the intrinsic parity of the state, negative for quark-antiquark states, positive for quark states, and negative for an antiquark plus gluon. Since partons’ momenta are generically not in the direction of \vec{P} , $k_{\perp} \neq 0$, one should remember that only *one* component of k_{\perp} changes sign under \hat{Y} . For $\Lambda = 0$, \hat{Y} turns the state to

itself, so for these states one can define Y -parity. The changed definition of parity completely changes the parity mixing rules, and respectively the number of light-front wave functions, as described in detail in [27].

Yet the light-front wave functions in the helicity basis, have different rules. The classification is not done via the total S_1, S_2, L : only their z components (meson directed) are used. They satisfy the obvious constraint

$$\Lambda = S_1^z + S_2^z + L^z.$$

In the following we will drop the z superscript. The $\Lambda = 0$ states are eigenstates of \hat{Y} , minus for pions and plus for rho mesons: those have two wave functions (see Appendix C) unlike $\Lambda = \pm 1$ states.

In [17] we focused on the spin-dependent forces, with $\vec{S}_1 \cdot \vec{S}_2, \vec{S} \cdot \vec{L}$ and tensor. Now we will have their analogs in beam projections, which we refer to by the same labels, without vectors. Some of them are nondiagonal. For instance, the tensor force can mix $|S_1 = S_2 = \frac{1}{2}, L = 0\rangle$ with $|S_1 = S_2 = -\frac{1}{2}, L = 2\rangle$.

B. General form of LFWFs for mesons with different Λ

To proceed with the spin effects, we need to get the full spin-orbit structure of the LFWFs. In order to explain what we mean, consider a meson with total *helicity* Λ (with longitudinal projection J_z). The total of two quark spins $\vec{S} = \vec{S}_1 + \vec{S}_2$ can be $S = 0$ or $S = 1$: in the former case $\Lambda = L_z$, and in the latter there are three cases: $L_z = \Lambda - 1, L_z = \Lambda, L_z = \Lambda + 1$. These four states (like e.g. χ_b, h_b) are in general mixed by spin-dependent forces. Schematically for the last three states, the mixing is captured by a 3×3 matrix (the index of ψ is the longitudinal projection of orbital momentum, or M_L)

$$H_{\Lambda} = (\psi_{\Lambda-1}, \psi_{\Lambda}, \psi_{\Lambda+1}) \begin{pmatrix} V_{\text{diag}} & V_{\pm 1} & V_{\pm 2} \\ V_{\pm 1} & V_{\text{diag}} & V_{\pm 1} \\ V_{\pm 2} & V_{\pm 1} & V_{\text{diag}} \end{pmatrix} \begin{pmatrix} \psi_{\Lambda-1} \\ \psi_{\Lambda} \\ \psi_{\Lambda+1} \end{pmatrix}. \quad (46)$$

The spin-orbit V_{SL} interaction changes L by ± 1 , and the tensor interaction V_T changes L by ± 2 . So, in general, any meson has *three wave functions*, mixed by spin- and $L_z = m$ -flipping forces.

For the important case of $\Lambda = 0$ —the pseudoscalar ($\eta_b \dots \pi$) and vector ($\Upsilon \dots \rho$)—is now diagonal. Thus these mesons have different parity. Furthermore, the two additional components involved are $\Lambda = \pm 1$, which by symmetry are the same [up to different factors $\exp(\pm i\phi)$]. So (as derived in [27]), one needs only *two* wave functions. Yet for consistency, for $\Lambda = 0$ we still define their wave functions with three components:

$$|P\rangle = \int d[1]d[2] \frac{\delta_{ij}}{\sqrt{N_c}} [\psi_0^P(x, k_{\perp}) (Q_{i\uparrow}^{\dagger}(1) \bar{Q}_{j\downarrow}^{\dagger}(2) - Q_{i\downarrow}^{\dagger}(1) \bar{Q}_{j\uparrow}^{\dagger}(2)) + \psi_{-1}^P(x, \vec{k}_{\perp}) Q_{i\uparrow}^{\dagger}(1) \bar{Q}_{j\uparrow}^{\dagger}(2) + \psi_{+1}^P(x, \vec{k}_{\perp}) Q_{i\downarrow}^{\dagger}(1) \bar{Q}_{j\downarrow}^{\dagger}(2)] |0\rangle, \quad (47)$$

$$\begin{aligned}
|V\rangle = & \int d[1]d[2] \frac{\delta_{ij}}{\sqrt{N_c}} [\psi_0^V(x, k_\perp) (Q_{i\uparrow}^\dagger(1) \bar{Q}_{j\downarrow}^\dagger(2) + Q_{i\downarrow}^\dagger(1) \bar{Q}_{j\uparrow}^\dagger(2)) \\
& + \psi_{-1}^V(x, \vec{k}_\perp) Q_{i\uparrow}^\dagger(1) \bar{Q}_{j\uparrow}^\dagger(2) - \psi_{+1}^V(x, \vec{k}_\perp) Q_{i\downarrow}^\dagger(1) \bar{Q}_{j\downarrow}^\dagger(2)] |0\rangle
\end{aligned} \quad (48)$$

with $N_c = 3$. The subscripts 0 and ± 1 on the wave functions refer to L_z , the z projections of the orbital momentum. Note that compared to the notations in [27], there are no explicit factors of $k_\perp^\pm = k_1 \pm ik_2$ here because they naturally belong to our wave functions, consistently defined not only for $m = L_z = 1$, but for any m value.

The $\Lambda = 0$ state of the vector mesons are called ‘‘transversely polarized.’’ The two other polarizations, with $\Lambda = \pm 1$ are ‘‘longitudinally’’ polarized. They are a bit more complicated, with three components each with different wave functions, corresponding to $L = 2, 1, 0$.

The invariant measure in (47) and (48) refers to the on-shell covariant one, with overall momentum conservation

$$d[1]d[2] = \frac{dx}{\sqrt{4x\bar{x}}} \frac{dp_\perp}{(2\pi)^3}. \quad (49)$$

Here x, \bar{x} are the fraction of longitudinal momenta carried by particle-1 and the antiparticle-2, or $x = p_1^+/P^+$ and $\bar{x} = p_2^+/P^+$ with $x + \bar{x} = 1$. The creation and annihilation operators in (47) and (48) obey the anticommutation rules

$$[Q_\alpha(k_1), Q_\beta^\dagger(k_2)]_+ = \delta_{\alpha\beta} 2k_1^+ (2\pi)^3 \delta(k_1^+ - k_2^+) \delta(k_{1\perp} - k_{2\perp})$$

for equal light-front time, so that the $|P, V\rangle$ states are covariantly normalized on the light front, e.g.

$$\langle P|P'\rangle = 2P^+ (2\pi)^3 \delta(P^+ - P'^+) \delta(P_\perp - P'_\perp). \quad (50)$$

It is readily checked that the light-front wave functions in (47) and (48) are normalized by

$$\int \frac{d^2k_\perp dx}{(2\pi)^3} (|\psi_0|^2 + |\psi_1|^2 + |\psi_{-1}|^2) = 1. \quad (51)$$

Below we show that ψ_0 refers to the twist-2 and $\psi_{\pm 1}$ to the (tensor) twist-3 contribution to the mesonic distribution amplitude.

VI. QUADRUPOLE MOMENT OF VECTOR MESONS AND $m \pm 2$ ‘‘TENSOR’’ MIXING

To explain why the effects of mixing spin and orbital momenta are important, let us take the classic example of the *quadrupole moment*. In the rest frame, these phenomena are well known in nuclear physics, for example the deuteron $d = pn$ state has total $J = 1$ and, in nonrelativistic notation, it is a mixture of $L = 0, J = 1$ and $L = 2, J = 1$ states induced by the tensor force.

In the light-front formulation, the rotational symmetry turns to a *hidden symmetry*, with apparent distinctions between longitudinal and transverse coordinates. Therefore, the LFWF mixing related to the quadrupole moment takes two different forms:

(1) for $\Lambda = 1$ it is mixing of $\Psi_{0,0}, \Psi_{0,2}$; and

(2) for $\Lambda = 0$ it is mixing of $\Psi_{0,-1}, \Psi_{0,1}$.

Note that the indices here are the quantum numbers n and m .

A. S-D mixing in the rest frame

To assess the S-D-shell (that is $L = 0$ to $L = 2$) mixing for Upsilon in the center of mass frame, we need to first consider the splitting due to the repulsive centrifugal potential ($6/r^2$) originating from the free Laplacian plus the Cornell potential, with the result

$$E_2 - E_0 = 0.46669 - (-0.47682) = 0.943 \text{ GeV}$$

(which is still subject to corrections by spin-dependent forces). This value is to be compared to the empirical mass difference

$$M_{\Upsilon 2} - M_{\eta_b} = 10.2325 - 9.3987 = 0.834 \text{ (GeV)}.$$

The S-D mixing requires two states with the same $J = 1$, which are constructed in a standard way, via Clebsch-Gordon coefficients

$$\psi_0^{M_J=1} = \psi_0(r) Y_{00}^1 \chi_1^1,$$

$$\psi_2^{M_J=1} = \psi_2(r) \left(\sqrt{\frac{3}{5}} Y_{20}^1 \chi_1^{-1} - \sqrt{\frac{3}{10}} Y_{21}^1 \chi_1^0 + \sqrt{\frac{1}{10}} Y_{22}^1 \chi_1^1 \right). \quad (52)$$

Here $Y_L^m(\theta, \phi)$ are spherical harmonics, and $\chi_S^{M_S}$ are states of total spin composed of Q and \bar{Q} . To proceed, we use the standard notation for the tensor force $V_T(r) S_{12}$, and the nondiagonal matrix element with the angular integral

$$\begin{aligned}
& \int d\Omega (Y_{00}^1 \chi_1^1) S_{12} \\
& \times \left(\sqrt{\frac{3}{5}} Y_{20}^1 \chi_1^{-1} - \sqrt{\frac{3}{10}} Y_{21}^1 \chi_1^0 + \frac{1}{\sqrt{10}} Y_{22}^1 \chi_1^1 \right) = \sqrt{8}. \quad (53)
\end{aligned}$$

As a result, the quadrupole moment is given by an integral

$$\begin{aligned}
\langle Q \rangle_\Upsilon &= \frac{\epsilon_{02}}{5\sqrt{2}} \int dr r^4 \Psi_{00}(r) \Psi_{02}(r) \\
&\approx \epsilon_{02} (0.14 \text{ GeV}^{-2}) \quad (54)
\end{aligned}$$

where the admixing amplitude of the D state is ϵ_{02} . If we assume it to be small, it is then given by the perturbative matrix element of the tensor mixing operator, sandwiched between states calculated using the Cornell potential

$$\epsilon_{02} = \frac{\sqrt{8} \int dr r^2 \Psi_{00}(r) V_{\pm 2}(r) \Psi_{02}(r)}{E_2 - E_0}. \quad (55)$$

For an estimate, we may use the perturbative contribution with

$$V_T(r) = \frac{4}{3} \frac{3\alpha_s}{r^3}. \quad (56)$$

B. Quadrupole moment of Upsilon meson from the light-front Hamiltonian

In this subsection we still consider the case of Υ , a vector meson made of a $\bar{b}b$ quark pair. In the rest frame we just discussed, the cases of transversely polarized $\Lambda = 0$ and longitudinally polarized $\Lambda = \pm 1$ are related by the $O(3)$ rotational symmetry. The matrix elements of the various tensor operators over the corresponding states are tied by the Wigner-Eckart theorem, and given by Clebsch-Gordon coefficients times a “reduced” (rotationally invariant) matrix element independent of the meson orientation.

In the light-front Hamiltonian H_{LF} in (36), the spin-tensor potential for heavy quarkonia comes from the last term with the instanton-induced effects (32). The spin operator can be rewritten in a more transparent way as

$$\begin{aligned} & \left(\sigma_{1\perp} \cdot \hat{b}_{21} \sigma_{2\perp} \cdot \hat{b}_{21} - \frac{1}{2} \sigma_{1\perp} \cdot \sigma_{2\perp} \right) \\ &= \frac{1}{4} (\sigma_{1-} \sigma_{2-} e^{2i\phi} + \sigma_{1+} \sigma_{2+} e^{-2i\phi}). \end{aligned} \quad (57)$$

The dependence on the azimuthal angle ϕ reflects on the mixing between the m and $m \pm 2$ states. We recall that the instanton contribution to the central potential was discussed in detail in [17], for the “dense instanton ensemble” with diluteness parameter κ set to one. The plot of the central potential $\mathbb{V}_C(\xi_x)$ and its second derivative $\mathbb{V}_C''(\xi_x)$ are given in Fig. 5. Note the change in sign at $b_\perp \sim 1.5 \text{ GeV}^{-1}$, a distance comparable to the size of Upsilon.

With our usual approximation for heavy quarkonia, $M \approx 2m_Q$ and $\xi_x \approx b_\perp$, its contribution to the mixing part of H_{LF} takes the form

$$\begin{aligned} & \langle n_1 m | V_{\pm 2} | n_2, m \pm 2 \rangle \\ &= \int d^2 b_\perp dx \Psi_{n_1 m}^* V_T(b_\perp) e^{-2i\phi} \Psi_{n_2 m \pm 2}. \end{aligned} \quad (58)$$

We show the factors depending on ϕ explicitly, but omit the spin operators.

To simplify the wave functions, let us for now ignore \tilde{V} in the Hamiltonian, which means using instead of $\Psi_{0,0}$, $\Psi_{0,2}$

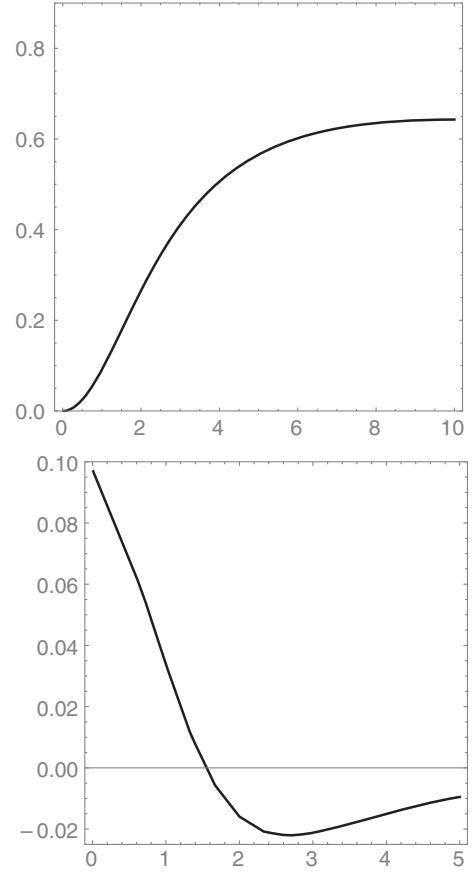


FIG. 5. The central part of the instanton induced potential $\mathbb{V}_C(\xi_x)$ versus the distance $\xi_x = r$ (top), and its second derivative $\mathbb{V}_C''(\xi_x)$ (bottom). See text.

LFWFs, the functions $\psi_{0,0}$, $\psi_{0,2}$ of the oscillator basis, (A3) and (C3). Recall that in the coordinate representation for the $\bar{b}b$ mesons, the size parameter $\beta \approx 0.62 \text{ GeV}$. The result is

$$\langle 00 | V_{\pm 2} | 0, 2 \rangle \approx -0.011 \text{ GeV}^2, \quad (59)$$

Note that if the size integral is split into the contributions stemming from the small plus large radial intervals, i.e. $[0, 1.5 \text{ GeV}^{-1}]$ plus $[1.5 \text{ GeV}^{-1}, \infty]$, we find 0.007 and -0.018 , respectively.

When (59) is divided by the difference of the mass squared for the two mixing states

$$\begin{aligned} \Delta M^2 &= M_{\Upsilon 2}^2 - M_{\eta_b}^2 \\ &= 10.2325^2 - 9.3987^2 \approx 16.4 \text{ GeV}^2 \end{aligned}$$

we get our estimates of the mixing parameter $\epsilon_{02} \approx 0.00064$. As a result, the estimate for the Upsilon quadrupole moment is then

$$Q_\Upsilon \sim 2\epsilon_{02} \int d^2 b_\perp dx \Psi_{0,0} \Psi_{0,2} b_\perp^2 \approx -0.0095 \text{ GeV}^2 \quad (60)$$

which means that the usually quoted combination is

$$Q_T M_T^2 \approx -0.87. \quad (61)$$

As we will see in the next subsection, it is right in the ballpark of other determination. Unfortunately, this result is relatively uncertain since it comes from significant cancellations of small and large ranges in the b_\perp -mixing integral. Deformations of the instantons—e.g. in instanton–anti-instanton “molecule” configuration described by streamline or thimble configuration—would change this number. Putting this observation into a positive direction, we may conclude that the quadrupole moments of mesons are sensitive to the exact nature of the nonperturbative vacuum fluctuations.

We recall that in [16], we extracted the matrix element of the tensor force from the masses of the P -wave states of mesons with different quark species, ranging from the heavy χ_b to the light K, π . We noted that this matrix element changes sign, in going from heavy to light mesons. This observation is consistent with the calculation of this section. This issue clearly deserves further studies.

C. Quadrupole moments of vector mesons from lattice and other approaches

There have been several lattice measurements of the quadrupole moments of vector mesons, and in all fairness we will not be able to cover them in this comparative study. In a recent lattice study of vector mesons composed of light, strange, and charmed quarks with $V = \rho, K^*, \rho_s, \rho_c$ (the latter carry artificial charge assignments), it was numerically found that $Q_V M_V^2 \approx -0.3$ [28], which is comparable to an earlier study with $Q_V M_V^2 \approx -0.23(2)$ [29]. When extrapolated to bottomium, the recent lattice result gives $Q_T \approx -0.003 \text{ GeV}^2$, with a mixing parameter $\epsilon_{02} \approx 0.02$ from our analysis.

Adhikari *et al.* [30] have used their version of light-front Hamiltonian and wave functions, and calculated form factors for the lowest states of charmonia and bottomonia. From Table V in [30], we see that their value for Upsilon is larger $Q_T M_T^2 = -0.731(9)$. In sum, the spread of these numbers is about a factor of 3, so the magnitude of the quadrupole moment of Upsilon remains relatively uncertain.

VII. GENERAL SPIN AND ORBIT MIXING FOR LIGHT QUARKS

So far, we have considered mixing between the $m = 0$ and $m = 2$ components of the quarkonia wave function by the tensor force $V_{\pm 2}$. Similarly, we can include spin-orbit force $V_{\pm 1}$ and spin-spin forces, generating the whole 3×3 mixing matrix. However, since we know that all mixing is suppressed by powers of the heavy quark mass, we can treat these mixings perturbatively and additively, as we did above.

Instead, we now switch to the more involved case of light quarks, where the mixing is not expected to be suppressed. Of course, this is well known from the spectroscopy in the rest frame: heavy quarkonia are nonrelativistic, while light quark systems are not. In the rest frame, it is difficult to compare these two limiting cases of the meson spectroscopy. Fortunately, in the light front the comparison is possible, as light and heavy quarks are treated democratically. The light-front Hamiltonian has the same form for both cases, with only few parameters due for change. The only special case is the pion as a Goldstone mode, that we will address in the next section (see also our qualitative analysis in [17]).

The “basic problem” of two constituent quarks connected by a confining string was already considered in [17]. There we did not yet have mixing of states with different (transverse) orbital momentum m , and considered only the set of functions with $m = 0$. The basis functions with $m \neq 0$ are discussed in Appendix C, including the transition from the momentum to the coordinate representation.

The general form of the mixing matrix H_Λ for a meson with helicity $\Lambda = J_z$ was already given in (46). The derivation of the perturbative and instanton-induced spin- and orbital- m -changing effects were given in our recent analysis in [17] and above. Our current task is to evaluate the corresponding matrix elements.

The diagonal in the m -part or V_{diag} consists of two parts, the one coming from the spinless $H_0 + \tilde{V}$ Hamiltonian and the one from the spin part. There is no need to describe in detail the former. In brief, the values of the squared masses for the $m = 0, 1, 2$ states were obtained after its diagonalization. Using the states detailed in the Appendix E, we get for the longitudinally polarized vector $\Lambda = 1$ case the following diagonal elements:

$$H_1^{00} = 2.229, \quad H_1^{11} = 2.833, \quad H_1^{22} = 3.434(\text{GeV}^2). \quad (62)$$

Three spin states $S = 1, S_z = 1, 0, -1$ are

$$|\uparrow\uparrow\rangle, \quad (|\uparrow\downarrow\rangle + |\downarrow\uparrow\rangle)/\sqrt{2}, \quad |\downarrow\downarrow\rangle,$$

respectively. The spin-spin forces are proportional to the same value $\langle \vec{S}_1 \cdot \vec{S}_2 \rangle = 1/4$, and the corresponding matrix elements of the perturbative (26) and instanton-induced (34) potentials with $|\Psi_{0m}\rangle^2$.

The near-diagonal $V_{\pm 1}$ part of the mixing matrix is due to the spin-orbit forces, from the perturbative (26) and instanton-induced effects (34). The former is proportional to $-\hat{S}_1 \cdot \hat{L}_2 + \hat{S}_2 \cdot \hat{L}_1$, in which $\hat{L}_2 = -\hat{L}_1$ so the two terms are added into the total spin \hat{S} . We only consider the nondiagonal operators $S^+ L^- + S^- L^+$ that flip the spin and m by ± 1 . The perturbative potential is $\sim 1/\xi_x^3$. If we ignore the longitudinal distance and use $\xi_x^2 \approx \vec{b}_\perp^2$, we may worry

about of the convergence of the integrand at the origin. In the transition between $m = 0$ and $m = 1$, one indeed finds a logarithmic divergence

$$\int d^2 b_{\perp} \Psi_{00} \frac{1}{b^3} \Psi_{01} \sim \int db_{\perp} b_{\perp} * \frac{1}{b_{\perp}^3} * b_{\perp} \sim \log(b_{\min}) \quad (63)$$

since at small b_{\perp} , $\Psi_{00} \sim b_{\perp}^0$, $\Psi_{01} \sim b_{\perp}$. This logarithmic divergence is cut off by the small longitudinal distance of about $\pi/M \approx \pi/2m_Q$. In contrast, in the transition between $m = 1$ and $m = 2$ the integral has $\Psi_{02} \sim b_{\perp}^2$ instead of Ψ_{00} , so it is convergent.

The instanton-induced spin-orbit contributes to the light-front Hamiltonian H_{LF} , with the corresponding potential $V'_C(\xi_x)$ shown in Fig. 6. It is regular at the origin, but with a relatively small range of about an instanton size $\sim 1.5 \text{ GeV}^{-1} \sim 0.3 \text{ fm}$.

The $V_{\pm 2}$ or tensor forces were discussed in detail above for the case of the transition between the $m = 0$ and $m = 2$

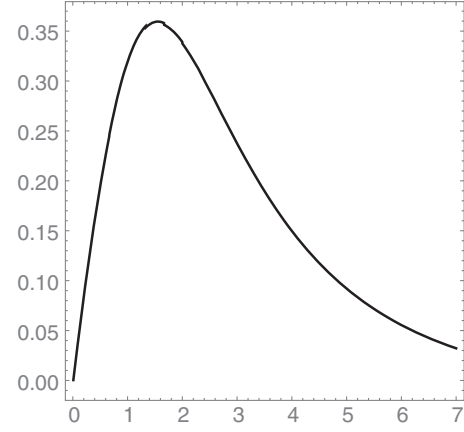


FIG. 6. Instanton-induced spin-orbit potential on the light-front $V'_C(\xi_x)$. See text.

states. The corresponding instanton-induced potential is shown in the bottom panel of Fig. 5.

After the evaluation of all matrix elements, we obtain the following mixing matrix:

$$H_{\Lambda=1} = \begin{pmatrix} M_0^2 + C^{00} + SS_C^{00} + SS_{\text{inst}}^{00}, & SL_C^{01} + SL_{\text{inst}}^{01}, & T_{\text{inst}}^{02} \\ SL_C^{01} + SL_{\text{inst}}^{01}, & M_1^2 + C^{11} + SS_C^{11} + SS_{\text{inst}}^{11}, & SL_{\text{pert}}^{12} + SL_{\text{inst}}^{12} \\ T_{\text{inst}}^{02}, & SL_{\text{pert}}^{12} + SL_{\text{inst}}^{12}, & M_2^2 + C^{22} + SS_C^{22} + SS_{\text{inst}}^{22} \end{pmatrix} \\ = \begin{pmatrix} 2.06789 & 0.289719 & -0.100297 \\ 0.289719 & 2.66282 & 0.0617886 \\ -0.100297 & 0.0617886 & 3.2959 \end{pmatrix}. \quad (64)$$

All entries in (64) are explained in Appendix D. The mixing changes the squared masses of the three $\Lambda = 1$ states as follows:

$$\{M_0^2, M_1^2, M_2^2\} = \{2.229, 2.833, 3.434\} \rightarrow \\ \{M_a^2, M_b^2, M_c^2\} = \{1.940, 2.779, 3.307\}.$$

The largest change is, as expected, a downward shift of the ground state.

One may think that the main shifts are due to Coulomb and spin-spin effects, and that the mixing is small. This is not the case, as one can see from the mixing coefficients associated to the wave functions for these three states

$$\Psi_a = 0.922252\psi_0 - 0.377037\psi_1 + 0.0854116\psi_2, \\ \Psi_b = 0.38106\psi_0 + 0.923825\psi_1 - 0.0365531\psi_2, \\ \Psi_c = -0.0651235\psi_0 + 0.0662586\psi_1 + 0.995675\psi_2.$$

There is significant 0-1 mixing due to spin-orbit interactions.

VIII. INCLUDING 't HOOFT EFFECTIVE LAGRANGIAN

The zero-mode contributions due to tunneling are captured by the 't Hooft determinantal interaction, in the rest frame. The 3-flavor determinantal interaction reduced to 2-flavor reads [16,17]

$$V_{TH}(1, 2) = -\frac{1}{4} |\tilde{\kappa}_2| A_{2N} (1 - \tau_1 \cdot \tau_2) \\ \times (1 - 16B_{2N} S_1 \cdot S_2) \delta(\vec{x}_{12}) \quad (65)$$

with the pair spatial distance $\vec{x}_{12} = \vec{x}_1 - \vec{x}_2$, in the ultralocal approximation for the instanton. However, the fermionic zero modes ride a nonlocal instanton tunneling process, and its interpretation in a boosted frame requires analytical continuation.

To derive the analog of (65) on the light front, we need to show how to analytically continue the fermionic tunneling process to the light front, where the in-out quarks are nearly on mass shell. We need an LSZ reduction scheme in *Euclidean signature* that extends to the light front in

Minkowski signature. For that, we follow the proposal suggested in [31].

A. LSZ reduction in the rest frame

For two flavors, the LSZ reduced 't Hooft vertex between on-shell light quarks in the rest frame is

$$\left\langle \left[\chi_R^\dagger(k_2) i k_2 \Phi_0(-k_2) \frac{1}{i m_q} \Phi_0^\dagger(k_1) i \bar{k}_1 \chi_L(k_1) \right] \times \left[\chi_R^\dagger(\underline{k}_2) i \underline{k}_2 \Phi_0(-\underline{k}_2) \frac{1}{i m_q} \Phi_0^\dagger(\underline{k}_1) i \bar{\underline{k}}_1 \chi_L(\underline{k}_1) \right] \right\rangle_U.$$

The averaging in (66) is over the $SU(N_c)$ color moduli U . Here each factor is on mass shell using the long time limit in Euclidean signature. More specifically, for the incoming left-handed and on-shell $\chi_L(k_1)$ going through an instanton, we define

$$\begin{aligned} & \Phi_0^\dagger(k_1) i k_1 \chi_L(k_1) e^{-|\vec{k}_1| |T|} \\ &= \lim_{T \rightarrow \infty} \int d^3 y \left(\frac{\rho^{\frac{3}{2}} U^\dagger \epsilon y \chi_L(k_1)}{y^4 \Pi_y^{\frac{3}{2}}} \right) e^{-i \vec{k}_1 \cdot \vec{y}} \end{aligned} \quad (66)$$

with $\Pi_y = 1 + \rho^2/y^2$ and $y = (-T, \vec{y})$. In the large Euclidean time limit $\Pi_y \rightarrow 1$, and the y integration reduces to

$$\lim_{T \rightarrow \infty} \int d^3 y \frac{-T \mathbf{1} - i \vec{\sigma} \cdot \vec{y}}{(T^2 + \vec{y}^2)^2 \Pi_y^{\frac{3}{2}}} e^{-i \vec{k}_1 \cdot \vec{y}} = \pi^2 (\mathbf{1} - \vec{\sigma} \cdot \hat{k}_1) e^{-|\vec{k}_1| |T|}. \quad (67)$$

Note the appearance of the mass-shell condition $E_1 = |\vec{k}_1|$ in the exponent, supporting the LSZ reduction in Euclidean signature. As a result, (66) simplifies to

$$\Phi_0^\dagger(k_1) i k_1 \chi_L(k_1) = (\pi \rho^{\frac{3}{2}}) [U^\dagger \epsilon (\mathbf{1} - \vec{\sigma} \cdot \hat{k}_1) \chi_L(k_1)] = (2\pi \rho^{\frac{3}{2}}) [U^\dagger \epsilon \chi_L(k_1)]. \quad (68)$$

Since $\chi_L(k_1)$ is left handed in the small current mass m_q limit, the right-most result follows. A repeat of this analysis yields (66) in the form

$$\left(\frac{4\pi^2 \rho^3}{i m_q} \right)^2 \langle [\chi_R^\dagger(k_2) \epsilon U] [U^\dagger \epsilon \chi_L(k_1)] \times [\chi_R^\dagger(\underline{k}_2) \epsilon U] [U^\dagger \epsilon \chi_L(\underline{k}_1)] \rangle_U. \quad (69)$$

B. LSZ reduction on the light front

To carry the preceding analysis to the light front, we first carry the analog of the LSZ reduction along $y_+ = \cos \theta y_4 + \sin \theta y_3$ for large y_+ in Euclidean signature, integrate over the remaining orthogonal directions $y_- = \sin \theta y_4 - \cos \theta y_3$ and y_\perp , and then analytically continue $\theta \rightarrow -i\chi$. More specifically, the analog of (67) is now

$$\begin{aligned} & \lim_{y_+ \rightarrow \infty} \int dy_- dy_\perp e^{-i k_{1-} y_- - i k_{1\perp} \cdot y_\perp} \left(\frac{[y_+ (\cos \theta - i \sin \theta \sigma_3) + y_- (\sin \theta + i \cos \theta \sigma_3) - i \sigma_\perp \cdot y_\perp]}{(y_+^2 + y_-^2 + y_\perp^2)^2 \Pi_y^{\frac{3}{2}}} \right) \\ &= \pi^2 \left((\cos \theta \mathbf{1} - i \sin \theta \sigma_3) - \frac{i k_{1-}}{k} (\sin \theta \mathbf{1} + i \cos \theta \sigma_3) - i \sigma_\perp \cdot y_\perp \right) e^{-k |y_+|} \end{aligned} \quad (70)$$

in the large y_+ limit, with

$$\begin{aligned} k_{1+} &= \cos \theta k_4 + \sin \theta k_3, \\ k_{1-} &= \sin \theta k_4 - \cos \theta k_3, \\ k &= (k_{1-}^2 + k_\perp^2)^{\frac{1}{2}}. \end{aligned} \quad (71)$$

The analytical continuation $\theta \rightarrow -i\chi$, $y_4 \rightarrow i y_0$ and $k_4 \rightarrow -i k_0$ yield (70) in the form

$$2\gamma \pi^2 (\mathbf{1} - \sigma_3) e^{-k |y_+|} \rightarrow \pi^2 (\mathbf{1} - \sigma_3) e^{-k |y_+|}. \quad (72)$$

Modulo the overall factor $2\gamma = 2P^+/M$ (to be absorbed in the new normalization of the states on the light front), (72) is compatible with (68) in the large momentum limit.

In retrospect, (72) shows that (69) extends to the light front in the form

$$\left(\frac{4\pi^2 \rho^3}{i m_q} \right)^2 \langle [\chi_{3R}^\dagger(k_2) \epsilon U] [U^\dagger \epsilon \chi_{3L}(k_1)] \times [\chi_{3R}^\dagger(\underline{k}_2) \epsilon U] [U^\dagger \epsilon \chi_{3L}(\underline{k}_1)] \rangle_U \quad (73)$$

with the L, R polarizations solely along the 3-direction. In other words, on the light front *helicity and chirality* are identified: a left-handed quark with spin down, flips to a right-handed quark with spin up as it tunnels through an instanton on the light front. The opposite flip takes place through an anti-instanton.

C. Zero mode induced ('t Hooft Lagrangian) interaction on the light front

Equation (73) does not carry any form factor in leading order, by the LSZ reduction. Its contribution to the invariant meson squared mass is

$$- \int \prod_{i=1}^2 \frac{dk_i^+}{4\pi k_i^+} \frac{d\bar{k}_i^+}{4\pi \bar{k}_i^+} \frac{dk_{i\perp}}{(2\pi)^2} \frac{d\bar{k}_{i\perp}}{(2\pi)^2} \times (2\pi)^3 2P^+ \delta(k_1^+ + \bar{k}_1^+ - k_2^+ - \bar{k}_2^+) \delta(k_{1\perp} + \bar{k}_{1\perp} - k_{2\perp} - \bar{k}_{2\perp}) \times \frac{n_{I+\bar{I}}}{2} \left(\frac{4\pi^2 \rho^3}{im_q} \right)^2 \langle [\chi_{3R}^\dagger(k_2) \epsilon U][U^\dagger \epsilon \chi_{3L}(k_1)] \times [\bar{\chi}_{3R}^\dagger(\bar{k}_2) \epsilon U][U^\dagger \epsilon \chi_{3L}(\bar{k}_1)] + L \leftrightarrow R \rangle_U \quad (74)$$

with the anti-instanton contribution added. Recall that in the rest frame, an effective form factor of the form (Euclidean signature)

$$(M(k_1)M(k_2)M(\bar{k}_1)M(\bar{k}_2))^{\frac{1}{2}} \rightarrow (M(k_{1\perp})M(k_{2\perp})M(\bar{k}_{1\perp})M(\bar{k}_{2\perp}))^{\frac{1}{2}} \quad (75)$$

is induced, with $M(k)$ the running constituent mass. Equation (75) regulates the momentum transfers, since the in-out quark pair is not on mass shell. We expect the right-most form factor in (75) to carry to the light front when the strict mass-shell limit is lifted as noted in [15,32].

The color averaging in (74) is similar to the color averaging carried in the rest frame (see Eq. (75) in [16]). The result for the bracket in the mesonic channel is

$$\begin{aligned} & [\bar{U}(k_2, s_2)U(k_1, s_1)\bar{V}(k_4, s_4)V(k_3, s_3) + \bar{U}(k_2, s_2)\gamma^5 U(k_1, s_1)\bar{V}(k_4, s_4)\gamma^5 V(k_3, s_3) \\ & - \bar{U}(k_2, s_2)\tau^a U(k_1, s_1)\bar{V}(k_4, s_4)\tau^a V(k_3, s_3) - \bar{U}(k_2, s_2)\gamma^5 \tau^a U(k_1, s_1)\bar{V}(k_4, s_4)\gamma^5 \tau^a V(k_3, s_3) \\ & - 4B_{2N}(\bar{U}(k_2, s_2)\sigma^a U(k_1, s_1)\bar{V}(k_4, s_4)\sigma^a V(k_3, s_3) + \bar{U}(k_2, s_2)\gamma^5 \sigma^a U(k_1, s_1)\bar{V}(k_4, s_4)\gamma^5 \sigma^a V(k_3, s_3) \\ & - \bar{U}(k_2, s_2)\sigma^a \tau^b U(k_1, s_1)\bar{V}(k_4, s_4)\sigma^a \tau^b V(k_3, s_3) - \bar{U}(k_2, s_2)\gamma^5 \sigma^a \tau^b U(k_1, s_1)\bar{V}(k_4, s_4)\gamma^5 \sigma^a \tau^b V(k_3, s_3)] \quad (76) \end{aligned}$$

with $U(k, s), V(k, s)$ the quark and the antiquark LF spinors respectively (see Appendix F). Note that the same interaction holds for

$$(\bar{U}U)(\bar{V}V) \rightarrow (\bar{U}V)(\bar{V}U)$$

through Fierz rearrangements.

Besides the standard flavor-determinantal character of the squared mass operator (74) after color averaging, its chief effect is to flip the helicity/chirality/spin of the in-out

nearly on-shell light-front quark pair, in the chiral limit. For three light flavors u, d, s in QCD, the arguments are similar, except that the strange quark loops in the sea are contracted as $\langle \bar{s}s \rangle < 0$. The reduction to two flavors u, d is structurally identical to (74), with only the overall coupling modified and *sign switched*.

On the LF, each of the contributions in (76) is spin valued. If we denote by $[s_2 s_1]$ the entries with s_1 for the initial spin and s_2 for the final spin, then the matrix valued forms are

$$\begin{aligned} \bar{U}_L(k_2, s_2)U_R(k_1, s_1) &= +\sqrt{k_1^+ k_2^+} \begin{pmatrix} \frac{m_{Q1}}{k_2^+} & 0 \\ \frac{k_{1R}}{k_1^+} - \frac{k_{2R}}{k_2^+} & \frac{m_{Q1}}{k_1^+} \end{pmatrix} = +\sqrt{x_1 x_2} \begin{pmatrix} \frac{m_{Q1}}{x_2} & 0 \\ \frac{k_{1R}}{x_1} - \frac{k_{2R}}{x_2} & \frac{m_{Q1}}{x_1} \end{pmatrix}, \\ \bar{U}_R(k_2, s_2)U_L(k_1, s_1) &= +\sqrt{k_1^+ k_2^+} \begin{pmatrix} \frac{m_{Q1}}{k_1^+} & \frac{k_{2L}}{k_2^+} - \frac{k_{1L}}{k_1^+} \\ 0 & \frac{m_{Q1}}{k_2^+} \end{pmatrix} = +\sqrt{x_1 x_2} \begin{pmatrix} \frac{m_{Q1}}{x_1} & \frac{k_{2L}}{x_2} - \frac{k_{1L}}{x_1} \\ 0 & \frac{m_{Q1}}{x_2} \end{pmatrix}, \end{aligned}$$

$$\begin{aligned}\bar{V}_L(k_1, s_1)V_R(k_2, s_2) &= -\sqrt{k_1^+k_2^+} \begin{pmatrix} \frac{m_{Q_2}}{k_2^+} & 0 \\ \frac{k_{1R}}{k_1^+} - \frac{k_{2R}}{k_2^+} & \frac{m_{Q_2}}{k_1^+} \end{pmatrix} = -\sqrt{x_1x_2} \begin{pmatrix} \frac{m_{Q_2}}{x_2} & 0 \\ \frac{k_{1R}}{x_1} - \frac{k_{2R}}{x_2} & \frac{m_{Q_2}}{x_1} \end{pmatrix}, \\ \bar{V}_R(k_1, s_1)V_L(k_2, s_2) &= -\sqrt{k_1^+k_2^+} \begin{pmatrix} \frac{m_{Q_2}}{k_1^+} & \frac{k_{2L}}{k_2^+} - \frac{k_{1L}}{k_1^+} \\ 0 & \frac{m_{Q_2}}{k_2^+} \end{pmatrix} = -\sqrt{x_1x_2} \begin{pmatrix} \frac{m_{Q_2}}{x_1} & \frac{k_{2L}}{x_2} - \frac{k_{1L}}{x_1} \\ 0 & \frac{m_{Q_2}}{x_2} \end{pmatrix},\end{aligned}\quad (77)$$

with $k_{1,2}^+ = x_{1,2}P^+$. For eikonized longitudinal momenta $k_1^+ \approx k_2^+$ commensurate with our use of the Wilson lines, (77) simplifies to

$$\begin{aligned}\bar{U}_L(k_2, s_2)U_R(k_1, s_1) &\rightarrow \begin{pmatrix} m_{Q_1} & 0 \\ \Delta_R & m_{Q_1} \end{pmatrix} = m_{Q_1}\mathbf{1} + \Delta_R\sigma^-, \\ \bar{U}_R(k_2, s_2)U_L(k_1, s_1) &\rightarrow \begin{pmatrix} m_{Q_1} & -\Delta_L \\ 0 & m_{Q_1} \end{pmatrix} = m_{Q_1}\mathbf{1} - \Delta_L\sigma^+, \\ \bar{V}_L(k_1, s_1)V_R(k_2, s_2) &\rightarrow \begin{pmatrix} -m_{Q_2} & 0 \\ \Delta_R & -m_{Q_2} \end{pmatrix} = -m_{Q_2}\mathbf{1} + \Delta_R\sigma^-, \\ \bar{V}_R(k_1, s_1)V_L(k_2, s_2) &\rightarrow \begin{pmatrix} -m_{Q_2} & -\Delta_L \\ 0 & -m_{Q_2} \end{pmatrix} = -m_{Q_2}\mathbf{1} - \Delta_L\sigma^+,\end{aligned}\quad (78)$$

with the momentum transfer $\Delta^\mu = k_1^\mu - k_2^\mu$, $\Delta_L = \Delta^1 - i\Delta^2 = \Delta_R^*$, and $\sigma^\pm = \frac{1}{2}(\sigma^1 \pm i\sigma^2)$. Inserting (78) into (76) yields the local determinantal two-body interaction potential (76) on the light front as

$$\begin{aligned}V_{TH}^{\eta'} &\approx -|\tilde{\kappa}_2|A_{2N}\frac{1}{4}(1 - \tau_1 \cdot \tau_2)[4m_{Q_1}m_{Q_2}\mathbf{1}_1\mathbf{1}_2 - 2(\sigma_{1\perp} \times \nabla_\perp m_{Q_2}\mathbf{1}_2 - m_{Q_1}\mathbf{1}_1\sigma_{2\perp} \times \nabla_\perp) \\ &\quad - (\sigma_{1\perp} \times \nabla_\perp)(\sigma_{2\perp} \times \nabla_\perp) - (\sigma_{1\perp} \cdot i\nabla_\perp)(\sigma_{2\perp} \cdot i\nabla_\perp)]\delta(P^+z^-)\delta(x_\perp)\end{aligned}\quad (79)$$

in the U(1) or η' channel, where only the leading $1/N_c$ contribution is shown. We have set

$$A_{2N} = \frac{2N_c - 1}{2N_c(N_c^2 - 1)}, \quad \tilde{\kappa}_2 = 3!G_{\text{Hooft}}\langle \bar{s}s \rangle < 0, \quad G_{\text{Hooft}} = \frac{n_{I+\bar{I}}}{2}(4\pi^2\rho^3)^3 \prod_{f=u,d,s} \frac{1}{m_f^*\rho}\quad (80)$$

with $\sigma_{i\perp}$ the \perp -Pauli matrices for particle $i = 1, 2$. The flavor permutation P_{12}^f is manifest in (76) as carried in (80)

$$\frac{1}{4}(1 - \tau_1 \cdot \tau_2) = \frac{1}{2}(1 - P_{12}^f).$$

This is just the projector on the flavor singlet states. This is at the origin of the famed 't Hooft determinantal interaction, which helps solve the U(1) problem for the 3-flavor case. [Note that the interaction is repulsive in the unprojected 3-flavor U(1) channel.]

Both spin contributions in (79) flip the spin of the incoming quark pair from L-down to R-up in the instanton contribution, and vice versa in the anti-instanton contribution. In the ultralocal approximation, we may trade $\nabla_\perp^2 \rightarrow 1/\rho^2$, hence the instanton induced spin-spin interaction in the 2-flavor singlet channel,

$$-|\tilde{\kappa}_2|A_{2N}\frac{1}{3}(1 - \tau_1 \cdot \tau_2)S_{1\perp} \cdot S_{2\perp}\delta(P^+z^-)\delta(x_\perp).\quad (81)$$

The nature of the instanton-induced interactions in the other meson channels with different spin flavor is manifest in the individual contributions in the Fierz form (76), with *no contribution* to the vector and pseudovector channels. For instance, in the pion channel, the light front interaction is

$$|\tilde{\kappa}_2|A_{2N}\frac{1}{3}\tau_1 \cdot \tau_2 S_{1\perp} \cdot S_{2\perp}\delta(P^+z^-)\delta(x_\perp)\quad (82)$$

which is attractive in the isospin-triplet and spin-singlet state, key for a massless pion. This point has been addressed in the literature many times before, including briefly in this series [17] (note that in the latter the interaction was assumed local in the invariant distance ξ_x for simplicity). If we were to treat this interaction perturbatively, it may appear that we should fit the magnitude of the four-fermion coupling constant to put the total pion mass to zero. However, this is not correct. This effect is dominant and leading in the pion channel, and

should not be treated perturbatively, as we showed qualitatively in [17]. For any large enough coupling (and thus instanton density) it breaks chiral symmetry and (in the chiral limit) produces exactly massless Nambu-Goldstone modes, the pions. Yet to show that quantitatively, we need to rederive the essentials of chiral symmetry breaking on the light front, a task we will discuss later in these series.

IX. VARIOUS OBSERVABLES

A. Parton distribution functions

The parton distributions functions or PDFs count the parton content of a given hadronic state. They are matrix elements of various operators sandwiched between pertinent light-front wave functions. For the hadronic states (47) and (48) limited to the lowest 2-particle wave-function contributions with net helicity zero, the pseudoscalar and vector PDFs are given by

$$q_{P,V}(x) = \int \frac{d^2 k_{\perp}}{(2\pi)^3} (|\psi_0^{P,V}|^2 + |\psi_1^{P,V}|^2 + |\psi_{-1}^{P,V}|^2) \quad (83)$$

with $q_{P,V}(\bar{x}) = q_{P,V}(x)$ for the antiparticles. The PDFs normalize to 1 using (51), which is the charge sum rule for a

given hadron. In the 2-particle approximation, the momentum sum rule is automatically fulfilled

$$\int_0^1 dx (xq_{P,V}(x) + \bar{x}q_{P,V}(\bar{x})) = 1. \quad (84)$$

B. Distribution amplitudes

The distribution amplitudes are defined as matrix elements of certain nonlocal operators on the light cone, sandwiched between the vacuum and pertinent hadronic states. They capture the longitudinal momentum and transverse location of a parton in the hadronic state.

DAs are widely used in the theory of hard exclusive reactions, such as the hadronic form factors in elastic scattering and heavy meson semileptonic decays. At high momentum transfer, factorization allows a split of the scattering amplitude into a ‘‘hard block operator,’’ sandwiched between two DAs. The moments of various DAs have been calculated on the lattice; for a reviews see [33].

The DAs are classified by the *twist* (dimension minus spin) of the operator involved. To give an example, since the early 1980s, most exclusive reactions involving the pions are based on the following three DAs:

$$\begin{aligned} & \int_{-\infty}^{+\infty} \frac{p^+ dz^-}{2\pi} e^{ixp \cdot z} \langle 0 | \bar{d}_{\beta}(0) [0, z] u_{\alpha}(z) | \pi^+(p) \rangle \\ &= \left(+ \frac{if_{\pi}}{4} \gamma^5 \left(\not{p} \varphi_{\pi^+}^A(x) - \chi_{\pi} \varphi_{\pi}^P(x) - i \chi_{\pi} \sigma_{\mu\nu} \frac{p^{\mu} n^{\nu}}{p \cdot n} \frac{\varphi_{\pi}^T(x)}{6} \right) \right)_{\alpha\beta} \end{aligned} \quad (85)$$

with n^{ν} a lightlike vector in the z direction. Note that although these matrix elements are nonlocal, the integral is just one dimensional, taken along the light-cone coordinate. The symbol $[x, y]$ is the shorthand notation for the gauge link between two points on the light front, and $\sigma_{\mu\nu} = \frac{1}{2i} [\gamma_{\mu}, \gamma_{\nu}]$. In this example the first term contains momentum, while the other two do not. Therefore the axial A -DA is of leading twist, while the two others P , T -DA are subleading (next twist) at large momentum $p \rightarrow \infty$.

The three functions $\varphi^i(x)$ have indices $i = A, P, T$ standing for axial, pseudoscalar, and tensor gamma matrices in the operator. They are all normalized to 1. Their explicit definition follows from (85) by inversion,

$$\begin{aligned} \varphi_{\pi^+}^A(x) &= \frac{1}{if_{\pi}} \int_{-\infty}^{+\infty} \frac{dz^-}{2\pi} e^{ixp \cdot z} \langle 0 | \bar{d}(0) \gamma^+ \gamma_5 [0, z] u(z) | \pi^+(p) \rangle, \\ \varphi_{\pi^+}^P(x) &= \frac{1}{f_{\pi} \chi_{\pi}} \int_{-\infty}^{+\infty} \frac{p^+ dz^-}{2\pi} e^{ixp \cdot z} \langle 0 | \bar{d}(0) i \gamma_5 [0, z] u(z) | \pi^+(p) \rangle, \\ \varphi_{\pi^+}^T(x) &= \frac{-6}{f_{\pi} \chi_{\pi}} \frac{p^{\mu} n^{\nu}}{p \cdot n} \int_{-\infty}^{+\infty} \frac{p^+ dz^-}{2\pi} e^{ixp \cdot z} \langle 0 | \bar{d}(0) \sigma_{\mu\nu} \gamma_5 [0, z] u(z) | \pi^+(p) \rangle. \end{aligned} \quad (86)$$

The constants DAs are normalized to 1. The axial pion DA is normalized by the weak pion decay constant $f_{\pi} \approx 133$ MeV, and the pseudoscalar and tensor pion DAs are normalized by χ_{π} which follows from the chiral algebra. These chiral parameters are a measure of the pion wave function at the origin of the *transverse plane* (zero transverse distance $b_{\perp} = 0$).

The DAs are only a function of the longitudinal momentum x .

1. Pion axial DA

To relate the pion axial DA in (86) to the pseudoscalar light-front wave function with helicity-0 in (47), we note the identity

$$\tau_{ud}^+ \left(\frac{1}{4} \gamma^5 \not{p} \right)_{\alpha\beta} = \frac{1}{2} \frac{1}{\sqrt{4x\bar{x}}} (u_{\alpha\uparrow}(1) \bar{d}_{\beta\downarrow}(2) - u_{\alpha\downarrow}(1) \bar{d}_{\beta\uparrow}(2)) \quad (87)$$

in the light-front limit. With this in mind, the leading twist-2 or axial distribution amplitude for $P = \pi^+$ (or any pseudo-scalar) in (86), matches the $m = 0$ contribution in (47)

$$\varphi_P^A(x) = \frac{2\sqrt{N_c}}{f_P} \int \frac{dk_\perp}{(2\pi)^3} \psi_0^P(x, k_\perp). \quad (88)$$

By the same reasoning, the corresponding contribution for the vectors, matches the $m = 0$ contribution in (48)

$$\varphi_V(x) = \frac{2\sqrt{N_c}}{f_V} \int \frac{dk_\perp}{(2\pi)^3} \psi_0^V(x, k_\perp). \quad (89)$$

2. Pion tensor DA

To relate the tensor pion DA amplitude in (86) to the pseudoscalar light-front wave function with helicity-1 in (47), we note that the dominant tensor matrix element on the light cone reads

$$\langle 0 | \bar{d}(0) i \sigma^{+i} \gamma_5 u(z^-, z_\perp) | \pi^+(p) \rangle = 2p^+ \frac{\partial}{\partial z_\perp^i} \psi_1^P(z^-, z_\perp) \quad (90)$$

with $(x = k^+ / p^+)$

$$\psi_1^P(x, k_\perp) = \int dz^- dz_\perp e^{i(k^+ z^- - k_\perp \cdot z_\perp)} \psi_1^P(z^-, z_\perp). \quad (91)$$

Note the relation $\psi_{\pm 1}^P(x, k_\perp) = k_\perp^\pm \psi_1^P(x, k_\perp)$ with $k_\perp^\pm = k_x \pm ik_y$. A comparison with (86) shows that the twist-3 pion distribution amplitude in $\varphi_T(x, k_\perp)$ matches the $m = 1$ contribution in (47) through

$$\frac{\partial}{\partial k_\perp^i} \varphi_T(x, k_\perp) = \frac{6}{f_\pi \chi_\pi} k_\perp^i \psi_1^P(x, k_\perp). \quad (92)$$

3. Bottomium DA

The generic LFWFs depend on all three variables x, b_\perp . The DAs are LFWF's at the origin in the coordinate representation, or the overall integral

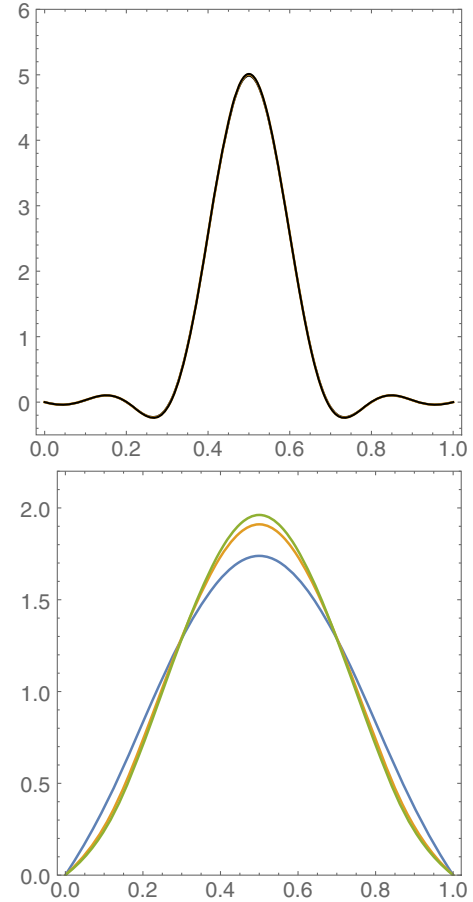


FIG. 7. Distribution amplitudes for $\bar{b}b$ (top) and a “generic” light $\bar{q}q$ meson (bottom) as a function of x , for the three lowest states $n = 0, 1, 2$. For bottomium, the difference between the three curves is too small to be visible. For the light meson, the differences are visible. With increasing n , the DAs become narrower and higher at $x = \frac{1}{2}$.

$$\Psi_{nm}(b_\perp = 0, x) = \int \frac{d^2 k_\perp}{(2\pi)^2} \Psi_{nm}(k_\perp, x) \quad (93)$$

in the momentum representation. They are normalized so that the integral over x is one. In Fig. 7 we show the DAs for $n = 0, 1, 2$ LFWFs, for $\bar{b}b$ and generic $\bar{q}q$ mesons. They look similar, but this only happens after integration over transverse momentum. For reference, the actual three functions (in our limited basis) look as follows:

$$\begin{aligned} \psi_0 &= e^{-7.14286\rho^2} ((-3.12914 + 1.86018\rho^2 - 0.72094\rho^4) \sin(\pi x) + (0.16657 + 0.636644\rho^2 - 0.490831\rho^4) \sin(3\pi x) \\ &\quad + (0.0267 + 0.111\rho^2 - 0.152\rho^4) \sin(5\pi x) + (0.00919 + 0.0402\rho^2 - 0.0577\rho^4) \sin(7\pi x)), \\ \psi_1 &= e^{-7.14286\rho^2} ((3.08754 - 48.5397\rho^2 + 20.882\rho^4) \sin(\pi x) + (-0.163697 + 2.98926\rho^2 + 5.18136\rho^4) \sin(3\pi x) \\ &\quad - (0.031 + 0.496\rho^2 + 0.347\rho^4) \sin(5\pi x) + (-0.011 + 0.170963\rho^2 + 0.118155\rho^4) \sin(7\pi x)), \\ \psi_2 &= e^{-7.142\rho^2} ((-2.79 + 82.46\rho^2 - 303.\rho^4) \sin(\pi x) + (0.242 - 9.649\rho^2 + 42.7\rho^4) \sin(3\pi x) \\ &\quad + (0.0403 - 1.272\rho^2 + 4.775\rho^4) \sin(5\pi x) + (0.0139 - 0.437\rho^2 + 1.64\rho^4) \sin(7\pi x)). \end{aligned}$$

Note first, that the heavier the meson, the slower the quark motion, with the DAs more concentrated near $x = \frac{1}{2}$. Note also that the bottomonia states with different orbital momenta m have practically the same DAs. Note finally that the oscillations in the DAs for bottomonia, are an artifact of the small basis set of functions in x that we used. Before normalization, the lowest bottomonium DA reads

$$DA(n=0, m=0) \sim (2.19 \sin(\pi x) - 1.79 \sin(3\pi x) + 1.16 \sin(5\pi x) - 0.44 \sin(7\pi x)).$$

with the trace referring to color spin. The generic pseudoscalar weak decay constant is then

$$f_P = 2\sqrt{N_c} \int \frac{dk_\perp}{(2\pi)^3} dx \psi_0^P(x, k_\perp). \quad (95)$$

Similar arguments applied to the weak decay constant of the $V = \rho^+$ meson defined as

$$\langle 0 | \bar{d}(0) \gamma^\mu u(0) | \rho^+(p) \rangle = \epsilon^\mu(p) m_\rho f_\rho \quad (96)$$

yield the generic vector decay constant

$$f_V = 2\sqrt{N_c} \int \frac{dk_\perp}{(2\pi)^3} dx \psi_0^V(x, k_\perp). \quad (97)$$

with $\varphi_\pi^P(x)$ normalized to 1. Using the Gell-Mann-Oakes-Renner relation

$$f_\pi^2 m_\pi^2 = -2(m_u + m_d) \langle \bar{q}q \rangle \quad (100)$$

with $|\langle \bar{q}q \rangle| \approx (240 \text{ MeV})^3$ yields

$$\chi_\pi = \frac{m_\pi^2}{(m_u + m_d)}. \quad (101)$$

C. Form factors

Elastic scattering is the simplest exclusive process, and the corresponding mesonic form factors have been studied extensively theoretically and experimentally, for about five decades. Here we do not have space for a review of their history; let us just say that early asymptotic predictions at

Note that the signs of the harmonics alternate, with a net effect being a suppression of the DA near the edges $x \rightarrow 0, 1$.

4. Decay constants

These matrix elements are best interpreted in the chiral basis. For the pseudoscalar pion, the leading twist-2 DA $\varphi_\pi(x)$ is *chirally diagonal*, but the subleading twist-3 are *chirally nondiagonal*. Fortunately, a matrix related the chiral basis to the spin basis has been already defined in the previous section.

The weak pion decay constant follows:

$$\langle 0 | \bar{d}(0) \gamma^\mu (1 - \gamma^5) u(0) | \pi^+(p) \rangle = -\text{Tr} \left(\gamma^\mu (1 - \gamma^5) \left(\frac{i}{4} \gamma^5 \not{p} \right) \right) 2 \int \frac{dk_\perp}{(2\pi)^3} \frac{dx}{\sqrt{N_c}} \psi_0^P(x, k_\perp) \equiv i f_\pi P^\mu \quad (94)$$

5. Chiral constant

Isospin symmetry and charge conjugation force $\varphi_\pi(x) = \varphi_\pi(\bar{x})$. As pointed out initially in [34], there are two twist-3 and *chirally nondiagonal* independent DA $\varphi_\pi^P(x)$ and $\varphi_\pi^T(x)$, characterizing the pseudoscalar and tensor strength in the pion respectively. The latter are tied by the current identity

$$\partial^\nu (\bar{d}(0) \sigma_{\mu\nu} \gamma_5 u(z)) = -\partial_\mu (\bar{d}(0) i \gamma_5 u(z)) + m \bar{d}(0) \gamma_\mu \gamma_5 u(z) \quad (98)$$

and share the same couplings. The value of the dimensional coupling constant χ_π can be fixed by the divergence of the axial-vector current and the partially conserved axial current relation

$$(m_u + m_d) \langle 0 | \bar{d}(0) i \gamma^5 u(0) | \pi^+(p) \rangle = -(m_u + m_d) \text{Tr} \left(i \gamma^5 \left(\frac{i f_\pi}{4} \gamma^5 \chi_\pi \right) \right) \int_0^1 dx \varphi_\pi^P(x) = (m_u + m_d) f_\pi \chi_\pi \quad (99)$$

large Q^2 , based on one-gluon exchange, are not yet met, neither in experiment or on the lattice.

[The “semihard” domain $Q^2 \sim \text{few GeV}^2$ is dominated by nonperturbative effects. In particular, in our previous paper [35], we have calculated the instanton-induced contributions to the hard block, and showed that they are comparable to the perturbative amplitudes. When combined, they reproduce the experimental/lattice data, provided that the diluteness parameter is not small $\pi^2 n_{I+\bar{I}} \rho^4 = O(1)$.]

On the light front, the form factors follow from the Drell-Yan-West construction using the good current $J^+ = J^0 + J^3$ [36,37]. The analog of the Breit frame with fixed energy in the rest frame is the Drell-Yan frame in the light-front frame, with fixed longitudinal momentum $P^+ = P'^+$, for $P' = P + q$ with spacelike squared momentum transfer $q^2 = -Q^2 = -q_\perp^2$. The key feature of this choice of current

and frame is that the vacuum production and annihilation diagrams are suppressed, and parton number is conserved in-out in the form factor viewed as a process $\gamma^* + P \rightarrow P'$.

For instance, the Drell-Yan-West form factor for charged pseudoscalars is helicity preserving with [36–38]

$$F_P(Q^2) = \langle P', 0, 0 | \frac{J^+(0)}{2P^+} | P, 0, 0 \rangle \\ = \int_0^1 dx \int \frac{dk_\perp}{(2\pi)^3} \psi_0^{P*}(x, k_\perp + \bar{x}q_\perp) \psi_0^P(x, k_\perp) \quad (102)$$

in the 2-particle approximation (low resolution). Similar expressions for the charged vectors can be derived. The thorough analyses of these form factors will be given in a sequel [18].

X. CONCLUSIONS

The chief aim of this series of papers is to *derive* the light-front Hamiltonian H_{LF} and corresponding wave functions from first principles, using the theoretical and empirical information we have at the moment. The important distinctions between our approach and other versions of H_{LF} in the literature are, among others, (i) our H_{LF} is not guessed, but derived using certain approximations; (ii) therefore we do not fit any of the parameters to the experimental data, rather we use the standard values for the quark masses, the string tension σ_T , the perturbative coupling α_s and the instanton ensemble parameters; (iii) we do not consider just one or two lowest states in each quark channel, but look for as many states as feasible, by relating the results to Regge behavior; and (iv) central to our derivation is the QCD vacuum as we know it, at low resolution.

In a wider perspective, these works continue to bridge light-front physics with the development in Euclidean space-time. The latter—lattice QCD simulations and semi-classical ensembles of instantons—have elucidated a rich vacuum structure dominated by inhomogeneous and topologically nontrivial gauge configurations. These configurations explain why chiral symmetry is spontaneously broken, and account for the emergence of mass through running quark effective masses.

A massless left-handed quark tunneling through an instanton emerges as a right-handed massless quark as a topological zero mode, a remarkable manifestation of the axial anomaly. This phenomenon is the essence of the dynamical breaking of chiral symmetry, which yields a running constituent mass. The collectivization of these zero modes is well understood from detailed numerical studies of instanton ensembles carried in the 1990s, and produces an octet of massless Nambu-Goldstone modes. The QCD vacuum possesses the zero mode zone with no gap near zero Dirac eigenvalue. In a way, we may say that the QCD vacuum is “metallic” with the scalar and vector mesons as weakly correlated “excitons.”

However, chiral symmetry breaking is not the only instanton-induced effect. Apart from well-isolated instantons

producing near-zero Dirac modes, there are also more numerous fluctuations which can be described as instanton–anti-instanton molecules. In the first paper of the series [16], we showed that by including them in Wilson line correlators, we can account for a significant part of the central interquark potential, as well as the spin-dependent potentials in heavy quarkonia.

The light-front observables at large normalization scale μ^2 paint a picture of hadrons containing multiple gluons, and a rich quark-antiquark sea. Yet at small resolution, of the order of $\mu \sim 1/\rho \approx 600$ MeV, we expect this picture to morph into the spectroscopic quark model, dominated by the minimal (2 for mesons, 3 for baryons) configurations. This is especially obvious for heavy quarkonia, which is the focus in this paper.

“Potentials” independent and dependent on spin variables are defined via certain *nonlocal* observables, such as the well-known Wilson lines. We know how to evaluate them in the Euclidean version of the QCD vacuum, on the lattice or when it can be regarded as a correlated ensemble of certain topological solitons, such as instantons and anti-instantons.

Bridging the Euclidean vacuum with the LF is one of the major challenges for theory today. In Paper II [17], we outlined a method to do so, by performing calculations in Euclidean space-time, and then analytically continuing *the results* (not the field configurations themselves). Wilson loop correlators are mapped on the light front, in terms of a slope angle θ in Euclidean signature, that is continued to $-i\chi$ (the rapidity) in Minkowski signature. This proposal was made long ago, and tested both at the perturbative [20] and nonperturbative [21,22] levels.

In a way, this proposal is different, although similar in spirit, to the large momentum effective approach [1], where Euclidean equal-time correlators are made to asymptote their light-cone counterparts. The large momentum limit in this case is analogous to the large rapidity $\theta \rightarrow -i\chi$ continuation in our case.

Finally, in this paper we explore the fortunate fact that on the light front, all hadrons—from bottomonia to the pions—can be approached from the same LF Hamiltonian. In the first approximation, it is just a transverse oscillator and longitudinal harmonic functions. In the next approximation, the nonfactorizable part \tilde{V} is included. For the lowest states, its influence is not too drastic.

The next approximation brings in the Coulomb, perturbative, and instanton-induced mixing, in spin and angular momenta. For heavy quarkonia these effects are suppressed by large quark masses. For light quark states, these effects are also not large, except for the ground states. The reason is that these mixing effects are short range. Narrow Wilson loops are mostly sensitive to the topologically active instanton and anti-instanton gauge configurations and chiral symmetry breaking. Wide Wilson loops are mostly sensitive to the flux disordering gauge vortices and confinement. Contrary to common lore, the QCD vacuum is

dominant on the light front too, and is central for the emergence of mass, confinement, and spin mixing.

The idea to derive *all* LF observables—DAs, PDFs, GPDs, form factors—from a common model Hamiltonian was put forth by Brodsky and his collaborators [39], and by Vary and his collaborators [40,41], with the intent to combine results of various experiments into a common framework. Their Hamiltonians were largely guessed, using insights from holographic QCD models.

Our approach is different. It is based on a derivation of a light-front Hamiltonian, from well-established features of the perturbative and nonperturbative QCD vacuum fields. We also used a wider set of states and quark masses, and showed that the excited states are much closer to the generic Regge trajectories. Indeed, for the excited states, the confining string becomes the only relevant physical effect, as explained in our introductory remarks in [16].

Looking at all works on H_{LF} , we believe that this is just the beginning of a successful modeling of hadrons on the light front, that factors in the wealth of information from the QCD vacuum. While our analyses deal solely with mesons, their generalization to baryons is relatively straightforward. Also, one can analyze multi-quark wave functions of mesons (tetraquarks) and baryons (pentaquarks), the antiquark sea, etc.

In many ways, the theoretical construction and tools presented and used in these serial analyses provide a common framework for both hadronic and nuclear physics.

ACKNOWLEDGMENTS

This work is supported by the Office of Science, U.S. Department of Energy under Contract No. DE-FG-88ER40388.

APPENDIX A: FUNCTIONAL BASIS USING A 2D OSCILLATOR HAMILTONIAN

Following our analysis in [17], we use the eigenfunction basis of the “2d oscillator” imbedded in part of the Hamiltonian H_0 in (37). We start by recalling its generic properties, and then use it either in the momentum or coordinate representation, whichever is more convenient.

The generic Hamiltonian is

$$H_{\text{osc}} = \vec{p}^2 \frac{1}{2\mu} + \vec{\rho}^2 \frac{\mu\omega^2}{2} \quad (\text{A1})$$

where $\vec{\rho}$ is a 2d coordinate, referred to as b_\perp in the main text. One way to generate all wave functions is to use two 1d oscillator notations, but a more convenient one is to use polar coordinates, so the Hamiltonian matrix consists of separate sectors of 3×4 size.

The basic LF Hamiltonian includes a diagonal H_0 and a nonfactorizable part

$$\tilde{V} = (M^2 + \vec{p}_\perp^2) \left(\frac{1}{x(1-x)} - 4 \right) \quad (\text{A2})$$

which can be calculated either in momentum or coordinate representations.

Note that the wave functions we use here are all normalized using

$$\int_0^1 dx \int d^2\rho_\perp \psi_{nm}^2(x, \rho_\perp) = 1,$$

which is natural in coordinate space. When used in momentum space, pertinent powers of $1/(2\pi)^3$ will be added whenever needed.

The wave functions which are independent of the azimuthal angle (angular momentum zero) will be used mostly in the momentum representation, with $\vec{\rho}$ as the transverse momentum. The orthonormal wave functions are

$$\begin{aligned} \{\psi_{n0}\} &= e^{-\beta^2 \rho^2/2} \sqrt{\frac{1}{\pi}} \beta \\ &\times \{1, (1 - \beta^2 \rho^2), (1 - 2\beta^2 \rho^2 + \beta^4 \rho^4/2), \dots\} \end{aligned} \quad (\text{A3})$$

with the β parameter given in terms of the Hamiltonian parameters $\beta = (4a/b/\sigma_T)^{1/4}$.

The harmonic set of orthonormal functions for longitudinal momentum fraction x , the set of functions $\chi_l(x)$, are labeled by *odd* integer $l = 1, 3, 5, \dots$,

$$\chi_l(x) = \sqrt{2} \{ \sin(\pi x), \sin(3\pi x), \sin(5\pi x), \sin(7\pi x), \dots \}. \quad (\text{A4})$$

The products of these two sets, define the set of states we used in our (angle-independent) calculations in the momentum representation.

The part of the Hamiltonian matrix used is thus limited by three maximal values of indices n, m, l , so the total size of the matrix is $N \times N$, with $N = n_{\text{max}} m_{\text{max}} l_{\text{max}}$. Obviously, the calculations significantly slow down with increasing N , and so for this exploratory paper we use a rather modest value of $N = 3 \times 3 \times 4$. Furthermore, before we account for mixing of states with different orbital momenta, m is conserved.

APPENDIX B: FROM BOTTOMONIUM TO GENERIC LIGHT MESONS, ON THE LIGHT FRONT

In our study in [17], we focused on the light quark systems on the light front. Here we start with the other extreme with the example of $\bar{b}b$ states, for which we use for the parameter $b = (2 * 4.8 \text{ GeV})^2$; $m_b = 4.8 \text{ GeV}$. In this section, we start with the states with zero angular momentum or $m = 0$. Our $M^2(a)$ curves lead to the selection of mass minima at about $a \approx 25$. With this in mind, we find the following 12 eigenvalues for the squared mass

$$M^2 \approx \{360., 341., 328., 169., 161., 153., 127., 121., 114., 113., 107., 101.\} \text{ (GeV}^2\text{)}.$$

The LFWF of the ground state is approximately factorized into

$$\Psi_{00} = e^{-1.302p_\perp^2} (-0.915 \sin(\pi x) + 0.749 \sin(3\pi x) - 0.485 \sin(5\pi x) + 0.183 \sin(7\pi x)) \quad (\text{B1})$$

where we have omitted all terms with coefficients smaller than 0.01. Note that the ground state is then the product of just a Gaussian in transverse momentum, times certain functions of x . However, the next eigenstates are not that simple. The LFWFs for the next two states with $n = 1, 2$ (and still independent on ϕ or for $m = 0$) are

$$\begin{aligned} \Psi_{10} = e^{-1.302\rho^2} & [(0.915 - 2.410\rho^2 + 0.025\rho^4) \sin(\pi x) + (-0.749 + 1.973\rho^2 - 0.018\rho^4) \sin(3\pi x) \\ & + (0.485 - 1.279\rho^2) \sin(5\pi x) + (-0.183 + 0.484\rho^2 - 0.0025\rho^4) \sin(7\pi x)], \end{aligned} \quad (\text{B2})$$

$$\begin{aligned} \Psi_{20} = e^{-1.302\rho^2} & [(0.905 - 4.726\rho^2 + 3.085\rho^4) \sin(\pi x) + (-0.741 + 3.876\rho^2 - 2.533\rho^4) \sin(3\pi x) \\ & + (0.480 - 2.521\rho^2 + 1.651\rho^4) \sin(5\pi x) - (0.182 + 0.957\rho^2 - 0.628\rho^4) \sin(7\pi x)]. \end{aligned} \quad (\text{B3})$$

Here $\rho^2 = \vec{p}_\perp^2$ (GeV²) and all coefficients are also in GeV units with appropriate powers. The Ψ_{n0} functions are eigenstates of H , and should not be confused with the basis set ψ_{nml} introduced above.

Their integrals of Ψ_{nm} over p_\perp give the DAs discussed in Sec. IX. Their x dependences are very similar. Their p_\perp dependence is shown in Fig. 8. In contrast to the x dependence, the p_T dependences are very different, as each curve reflects on the proper number of n zeros.

The same construction for generic light quarks with $m_q = 0.35$ GeV was discussed in [17]. Here, we slightly

modify the setting by selecting the variational minima at $a = 4$. The p_\perp dependence of the first three states is shown in Fig. 8.

For reference, the squared masses of the 12 lowest eigenvalues are

$$M^2 = 26.20, 23.70, 21.92, 15.77, 13.87, 12.28, \\ 8.79, 7.21, 5.77, 4.63, 3.43, 2.23 \text{ (GeV}^2\text{)}$$

and the lowest wave function is

$$\begin{aligned} \Psi_{00} = e^{-7.14286\rho^2} & (-3.12914 + 1.86018\rho^2 - 0.72094\rho^4) \sin(\pi x) \\ & + (0.16657 + 0.636644\rho^2 - 0.490831\rho^4) \sin(3\pi x) \\ & + 0.0267555 \sin(5\pi x) + 0.111208\rho^2 \sin(5\pi x) - 0.152454\rho^4 \sin(5\pi x) \\ & + 0.00919945 \sin(7\pi x) + 0.0402368\rho^2 \sin(7\pi x) - 0.0577019\rho^4 \sin(7\pi x). \end{aligned} \quad (\text{B4})$$

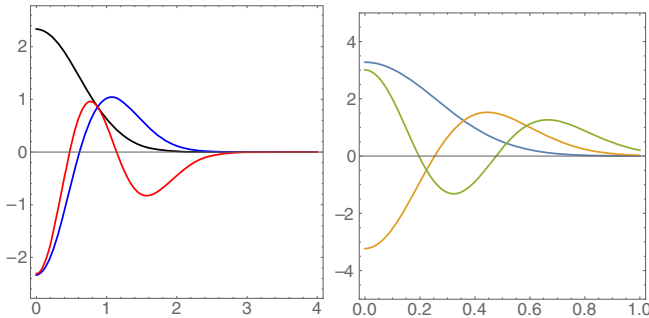


FIG. 8. Three lowest LFWFs with $n = 0, 1, 2, m = 0$ as a function of p_\perp (GeV) at $x = \frac{1}{2}$, for bottomonium (left) and a typical light meson (right). The number of zeros are commensurate with n .

APPENDIX C: WAVE FUNCTIONS WITH NONZERO ANGULAR MOMENTUM $L_z = m$

The functions with nonzero orbital momentum m are generated by the corresponding right (plus) creation operators

$$\begin{aligned} a_R^\dagger &= \frac{1}{2} e^{i\phi} \left(\beta\rho - \frac{1}{\beta} \frac{\partial}{\partial\rho} - \frac{i}{\beta\rho} \frac{\partial}{\partial\phi} \right), \\ a_L^\dagger &= \frac{1}{2} e^{-i\phi} \left(\beta\rho - \frac{1}{\beta} \frac{\partial}{\partial\rho} + \frac{i}{\beta\rho} \frac{\partial}{\partial\phi} \right), \end{aligned} \quad (\text{C1})$$

and the needed extra factors for proper wave function normalization $1/\sqrt{n_R!n_L!}$ depending on the numbers of right- and left-rotating “quanta.”

In particular, we use the following orthonormal sets of functions ψ_{nm} depending on ρ and azimuthal angle ϕ , with principle quantum number $n = 0, 1, 2, \dots$ and angular momentum $m = 0, 1, 2, \dots$

$$\{\psi_{01}\} = e^{-\beta^2 \rho/2 + i\phi} \sqrt{\frac{1}{\pi}} \beta^2 \rho \times \{1, (-2 + \beta^2 \rho^2)/\sqrt{2}, (6 - 6\beta^2 \rho^2 + \beta^4 \rho^4)/2\sqrt{3}, \dots\}, \quad (\text{C2})$$

$$\{\psi_{02}\} = e^{-\beta^2 \rho^2/2 + 2i\phi} \sqrt{\frac{1}{2\pi}} \beta^3 \rho^2 \times \left\{1, (3 - \beta^2 \rho^2)/\sqrt{3}, (12 - 8\beta^2 \rho^2 + \beta^4 \rho^4) \frac{\sqrt{2}}{4\sqrt{3}}, \dots\right\}. \quad (\text{C3})$$

When matrix elements of some potentials are evaluated, it is more natural to switch to the coordinate representation. One way to do so is to rederive an oscillatory basis in which $\rho^2 = \vec{r}_\perp^2$ and \vec{p}^2 is interpreted as a Laplacian containing an angular (centrifugal) term. In this case, the parameter β is inverted. A simpler way is to go to coordinate representation by 2d Fourier transform. While doing so, it is convenient to return to Cartesian coordinates, e.g. $\rho e^{\pm i\phi} \rightarrow p_x \pm ip_y$, which after double Fourier transform produce factors $x \pm iy$. With slight abuse of notation, we write the latter combination as $re^{\pm i\phi}$, although the angles ϕ in momentum and coordinate representations do not have the same meaning. Also note that in coordinate

representation one may better use the *inverted* scale parameter

$$\beta_p \rightarrow \beta_r = \frac{1}{\beta_p} = \left(\frac{4a}{b\sigma_T}\right)^{\frac{1}{4}}.$$

Recall that a is to be determined from the mass minimization, $b = M_{\text{mes}}^2 \approx (2m_Q)^2$, and the string tension is standard $\sigma_T = (0.4 \text{ GeV})^2$. Note also that, as expected, the wave functions at small distances are $\sim \rho^m$.

Now we return to the momentum representation and diagonalize $H_0 + \tilde{V}$ for $m = 1, 2$. For the bottomonium parameters the list of the six lowest squared masses are

$$M_{0,\pm 1}^2 = \{131.1, 124.4, 117.8, 116.6, 110.4, 104.2\},$$

$$M_{0,\pm 2}^2 = \{134.4, 127.7, 121.1, 119.7, 113.5, 107.3\},$$

$$\begin{aligned} \Psi_{01} = & e^{-1.30\rho^2} \rho e^{\pm i\phi} [(1.48 - 0.015\rho^2) \sin(\pi x) \\ & + (-1.21 + 0.011\rho^2) \sin(3\pi x) + 0.787 \sin(5\pi x) - 0.298 \sin(7\pi x)], \end{aligned} \quad (\text{C4})$$

$$\Psi_{02} = e^{-1.30\rho^2} \rho^2 e^{\pm 2i\phi} [1.67 \sin(\pi x) \quad (\text{C5})$$

$$- 1.37 \sin(3\pi x) + 0.89 \sin(5\pi x) - 0.34 \sin(7\pi x)]. \quad (\text{C6})$$

APPENDIX D: MIXING MATRIX ELEMENTS

In (64) we defined the 3×3 mixing matrix between states with different azimuthal quantum numbers $m = 0, 1, 2$, for a meson with fixed helicity $\Lambda = 1$. For simplicity, we did not use the states $\Psi_{nm}(x, \vec{k}_\perp)$ determined in the previous section, but rather the basic and simple oscillatory states $\psi_{nm}(k_\perp)$. These states carry the azimuthal dependence through $e^{im\phi}$, and the x dependence through $\sqrt{2} \sin(n\pi x)$, which are standard and not explicitly shown.

In this simplified basis, the Coulomb interaction

$$2MV_C = 2M_{\text{mes}} \left(-\frac{4\alpha_S}{3\rho} \right)$$

is diagonal

$$C^{mm} = \int_0^\infty |\psi_{0m}|^2 V_C(\rho) 2\pi\rho d\rho. \quad (\text{D1})$$

For $m = \{0, 1, 2\}$, the entries are explicitly

$$C^{mm} = M_{\text{mes}} \sqrt{\pi} \alpha_S \beta \{-8/3, -4/3, -1\}.$$

Note that here we use the coordinate representation and the oscillator parameter β , the inverse of the oscillator parameter in the momentum representation.

The perturbative spin-spin interaction is $\vec{S}_1 \vec{S}_2 = \frac{1}{4}$, for the states with total spin $S = 1$, so that $S_{1\perp} S_{2\perp} = \frac{2}{3} \frac{1}{4}$. Its associated transverse Coulomb potential ∇_\perp^2 / ρ is regulated at short distances, through

$$V_{\text{pert}}^{SS} = \frac{2}{3} \frac{1}{4} \left(\frac{2M_{\text{mes}}}{m_q^2} \right) \left(-\frac{4\alpha_S}{3} \right) \nabla_{\perp}^2 \frac{1}{\sqrt{\rho^2 + \epsilon^2}}$$

$$= -\frac{4M_{\text{mes}}\alpha_S}{9m_q^2} \frac{-2\epsilon^2 + \rho^2}{(\epsilon^2 + \rho^2)^{5/2}}. \quad (\text{D2})$$

In the limit $\epsilon \rightarrow 0$, it reduces to

$$SS_{\text{pert}}^{mm} = \frac{2M_{\text{mes}}\sqrt{\pi}\alpha_S\beta^3}{m_q^2} \{4/9, -2/9, -1/18\}$$

for $m = \{0, 1, 2\}$

The induced instanton spin-spin, spin-orbit, and tensor forces cannot be carried analytically. We evaluated them numerically, using the potentials shown in Figs. 5 and 6, as explained in the text. The numerics are carried for light quarks with mass $m_q = 0.35$ GeV and $M_{\text{mes}} = 2m_q$. The matrix elements are integrals of these potentials times the pertinent wave functions ψ_{0m} , $m = 0, 1, 2$ in coordinate space. The results are given in the second line of (64).

APPENDIX E: SPIN, HELICITY, AND CHIRALITY SPINORS

The light-front wave functions in [12] are built in terms of the spin and angular momentum projected along the z direction, which is the *hadron* momentum \vec{P} direction. In the case of mesons, there are two sets of spin variables $S_{Q,\bar{Q}} = S_{1,2}$ and a single orbital momentum L .

Let the direction of the quark momentum be described by standard polar angles θ, ϕ , with $p_{\perp} = P \sin(\theta)$ etc. In this case the spin up and down basis (with standard Dirac matrices) is

$$|\text{spin}\uparrow\rangle = \sqrt{\frac{E+m}{2m}} \times \begin{bmatrix} 1 \\ 0 \\ \frac{p}{E+m} \cos(\theta) \\ \frac{p}{E+m} \sin(\theta) e^{i\phi} \end{bmatrix}, \quad (\text{E1})$$

$$|\text{spin}\downarrow\rangle = \sqrt{\frac{E+m}{2m}} \times \begin{bmatrix} 0 \\ 1 \\ \frac{p}{E+m} \sin(\theta) e^{-i\phi} \\ \frac{p}{E+m} \cos(\theta) \end{bmatrix}. \quad (\text{E2})$$

The helicity $\lambda = \vec{S} \cdot \vec{k}$ defines a different basis, because the spin projection is defined not along the incoming z axis but along the quark momentum. Of course, quarks in the hadron have nonzero transverse components to it, $|p_{\perp}| = p \sin(\theta)$. The nonrelativistic 2-component spinors with $\lambda = \pm 1$ are obtained by rotation

$$h_{+} = (\cos(\theta/2), e^{i\phi} \sin(\theta/2)),$$

$$h_{-} = (-\sin(\theta/2), e^{i\phi} \cos(\theta/2)), \quad (\text{E3})$$

and, after a boost, the corresponding Dirac spinors are

$$|h_{+}\rangle = \sqrt{\frac{E+m}{2m}} \times \begin{bmatrix} \cos(\theta/2) \\ \sin(\theta) e^{i\phi} \\ \frac{p}{E+m} \cos(\theta/2) \\ \frac{p}{E+m} \sin(\theta/2) e^{i\phi} \end{bmatrix}, \quad (\text{E4})$$

$$|h_{-}\rangle = \sqrt{\frac{E+m}{2m}} \times \begin{bmatrix} -\sin(\theta/2) \\ \cos(\theta/2) e^{-i\phi} \\ \frac{p}{E+m} \sin(\theta/2) \\ -\frac{p}{E+m} \cos(\theta/2) e^{-i\phi} \end{bmatrix}. \quad (\text{E5})$$

We will also use the chiral basis, which is obtained from the helicity basis by taking the ultrarelativistic limit [$m \rightarrow 0$, $p/(E+m) \rightarrow 1$] inside the spinor

$$|c_{+}\rangle = \sqrt{\frac{E+m}{2m}} \times \begin{bmatrix} \cos(\theta/2) \\ \sin(\theta) e^{i\phi} \\ \cos(\theta/2) \\ \sin(\theta/2) e^{i\phi} \end{bmatrix}, \quad (\text{E6})$$

$$|c_{-}\rangle = \sqrt{\frac{E+m}{2m}} \times \begin{bmatrix} -\sin(\theta/2) \\ \cos(\theta/2) e^{-i\phi} \\ \sin(\theta/2) \\ -\cos(\theta/2) e^{-i\phi} \end{bmatrix}, \quad (\text{E7})$$

so that they become eigenvectors of the chiral projectors $P_{\pm} = (1 \pm \gamma_5)/2$.

Having specified these spinors, one can define the matrices rotating one set to the other. In particular, the transition between the spin and helicity states, takes the simple form

$$\frac{\langle s\uparrow|h_{+}\rangle}{\langle h_{+}|h_{+}\rangle} = \cos(\theta/2), \quad \frac{\langle s\downarrow|h_{+}\rangle}{\langle h_{+}|h_{+}\rangle} = \sin(\theta/2) e^{i\phi},$$

$$\frac{\langle s\uparrow|h_{-}\rangle}{\langle h_{-}|h_{-}\rangle} = -\sin(\theta/2), \quad \frac{\langle s\downarrow|h_{-}\rangle}{\langle h_{-}|h_{-}\rangle} = \cos(\theta/2) e^{i\phi}, \quad (\text{E8})$$

which—in the ultrarelativistic limit—is the same as the matrix between the spin basis and chirality basis.

APPENDIX F: LF DIRAC SPINORS

The LF Dirac spinors used to derive (77) are for the L -quark spinor with mass m_{Q_1}

$$\begin{aligned}
U_L(k, \uparrow) &= \frac{1}{(\sqrt{2}k^+)^{\frac{1}{2}}} \begin{pmatrix} m_{Q_1} \\ -k_R \end{pmatrix}, \\
U_L(k, \downarrow) &= \frac{1}{(\sqrt{2}k^+)^{\frac{1}{2}}} \begin{pmatrix} -k_L \\ \sqrt{2}k^+ + \frac{1}{2}m_{Q_1} \end{pmatrix}, \quad (\text{F1})
\end{aligned}$$

and the R -quark spinor with the same mass

$$\begin{aligned}
U_R(k, \uparrow) &= \frac{1}{(\sqrt{2}k^+)^{\frac{1}{2}}} \begin{pmatrix} \sqrt{2}k^+ + \frac{1}{2}m_{Q_1} \\ k_R \end{pmatrix}, \\
U_R(k, \downarrow) &= \frac{1}{(\sqrt{2}k^+)^{\frac{1}{2}}} \begin{pmatrix} k_L \\ m_{Q_1} \end{pmatrix}. \quad (\text{F2})
\end{aligned}$$

For the L -antiquark spinor with mass m_{Q_2} , we have

$$\begin{aligned}
V_L(k, \uparrow) &= \frac{1}{(\sqrt{2}k^+)^{\frac{1}{2}}} \begin{pmatrix} -k_L \\ \sqrt{2}k^+ + \frac{1}{2}m_{Q_2} \end{pmatrix}, \\
V_L(k, \downarrow) &= \frac{1}{(\sqrt{2}k^+)^{\frac{1}{2}}} \begin{pmatrix} -m_{Q_2} \\ k_R \end{pmatrix}, \quad (\text{F3})
\end{aligned}$$

and for the R antiquark with the same mass

$$\begin{aligned}
V_R(k, \uparrow) &= \frac{1}{(\sqrt{2}k^+)^{\frac{1}{2}}} \begin{pmatrix} -k_L \\ -m_{Q_2} \end{pmatrix}, \\
V_R(k, \downarrow) &= \frac{1}{(\sqrt{2}k^+)^{\frac{1}{2}}} \begin{pmatrix} \sqrt{2}k^+ + \frac{1}{2}m_{Q_2} \\ k_R \end{pmatrix}. \quad (\text{F4})
\end{aligned}$$

-
- [1] X. Ji, *Phys. Rev. Lett.* **110**, 262002 (2013).
[2] J.-H. Zhang, J.-W. Chen, X. Ji, L. Jin, and H.-W. Lin, *Phys. Rev. D* **95**, 094514 (2017).
[3] C. Alexandrou, K. Cichy, M. Constantinou, K. Jansen, A. Scapellato, and F. Steffens, *Phys. Rev. Lett.* **121**, 112001 (2018).
[4] Y. Nambu and G. Jona-Lasinio, *Phys. Rev.* **122**, 345 (1961).
[5] J. J. M. Verbaarschot and I. Zahed, *Phys. Rev. Lett.* **70**, 3852 (1993).
[6] G. Montambaux, *Phys. Rev. B* **55**, 12833 (1997).
[7] S. J. Brodsky and R. Shrock, *Proc. Natl. Acad. Sci. U.S.A.* **108**, 45 (2011).
[8] S. J. Brodsky, C. D. Roberts, R. Shrock, and P. C. Tandy, *Phys. Rev. C* **85**, 065202 (2012).
[9] G. F. De Téramond and S. J. Brodsky, *Phys. Rev. D* **104**, 116009 (2021).
[10] X. Ji, *Nucl. Phys.* **B960**, 115181 (2020).
[11] X. Ji, Y.-S. Liu, Y. Liu, J.-H. Zhang, and Y. Zhao, *Rev. Mod. Phys.* **93**, 035005 (2021).
[12] X.-d. Ji, J.-P. Ma, and F. Yuan, *Nucl. Phys.* **B652**, 383 (2003).
[13] C. Shi, C. Chen, L. Chang, C. D. Roberts, S. M. Schmidt, and H.-S. Zong, *Phys. Rev. D* **92**, 014035 (2015).
[14] C. Shi and I. C. Cloet, *Phys. Rev. Lett.* **122**, 082301 (2019).
[15] A. Kock and I. Zahed, *Phys. Rev. D* **104**, 116028 (2021).
[16] E. Shuryak and I. Zahed, this issue, *Phys. Rev. D* **107**, 034023 (2023).
[17] E. Shuryak and I. Zahed, preceding paper, *Phys. Rev. D* **107**, 034024 (2023).
[18] E. Shuryak and I. Zahed, following paper, *Phys. Rev. D* **107**, 034026 (2023).
[19] E. Shuryak and I. Zahed, this issue, *Phys. Rev. D* **107**, 034027 (2023).
[20] E. Meggiolaro, *Eur. Phys. J. C* **4**, 101 (1998).
[21] E. V. Shuryak and I. Zahed, *Phys. Rev. D* **62**, 085014 (2000).
[22] M. Giordano and E. Meggiolaro, *eCONF C0906083*, 31 (2009).
[23] R. A. Janik and R. B. Peschanski, *Nucl. Phys.* **B586**, 163 (2000).
[24] G. Basar, D. E. Kharzeev, H.-U. Yee, and I. Zahed, *Phys. Rev. D* **85**, 105005 (2012).
[25] E. Shuryak and I. Zahed, *Ann. Phys. (Amsterdam)* **396**, 1 (2018).
[26] M. Musakhanov and U. Yakhshiev, *Int. J. Mod. Phys. E* **30**, 2141005.
[27] X.-d. Ji, J.-P. Ma, and F. Yuan, *Eur. Phys. J. C* **33**, 75 (2004).
[28] Y.-Z. Xu, D. Binosi, Z.-F. Cui, B.-L. Li, C. D. Roberts, S.-S. Xu, and H. S. Zong, *Phys. Rev. D* **100**, 114038 (2019).
[29] J. J. Dudek, R. G. Edwards, and D. G. Richards, *Phys. Rev. D* **73**, 074507 (2006).
[30] L. Adhikari, Y. Li, M. Li, and J. P. Vary, *Phys. Rev. C* **99**, 035208 (2019).
[31] Y. Liu and I. Zahed, [arXiv:2102.07248](https://arxiv.org/abs/2102.07248).
[32] A. Kock, Y. Liu, and I. Zahed, *Phys. Rev. D* **102**, 014039 (2020).
[33] V. M. Braun, S. Collins, M. Göckeler, P. Pérez-Rubio, A. Schäfer, R. W. Schiel, and A. Sternbeck, *Proc. Sci. QCDEV2015 (2015)* 009 [[arXiv:1510.07429](https://arxiv.org/abs/1510.07429)].
[34] B. Geshkenbein and M. Terentev, *Phys. Lett.* **117B**, 243 (1982).
[35] E. Shuryak and I. Zahed, *Phys. Rev. D* **103**, 054028 (2021).
[36] S. D. Drell and T.-M. Yan, *Phys. Rev. Lett.* **24**, 181 (1970).
[37] G. B. West, *Phys. Rev. Lett.* **24**, 1206 (1970).
[38] G. P. Lepage and S. J. Brodsky, *Phys. Rev. D* **22**, 2157 (1980).
[39] S. J. Brodsky, G. F. de Téramond, H. G. Dosch, and J. Erlich, *Phys. Rep.* **584**, 1 (2015).
[40] Y. Li, P. Maris, X. Zhao, and J. P. Vary, *Phys. Lett. B* **758**, 118 (2016).
[41] C. Mondal, J. Lan, K. Fu, S. Xu, Z. Hu, X. Zhao, and J. P. Vary, *SciPost Phys. Proc.* **10**, 036 (2022).